IEEE Access
Multidisciplinary | Rapid Review | Open Access Journal

Received 23 August 2023, accepted 15 December 2023, date of publication 22 December 2023,
date of current version 16 January 2024.

Digital Object Identifier 10.1109/ACCESS.2023.3346039

RESEARCH ARTICLE

Self-Optimization of Handover Control Parameters for 5G Wireless Networks and Beyond

ABBAS IBRAHIM MBULWA, (Graduate Student Member, IEEE), HOE TUNG YEW, (Member, IEEE), ALI CHEKIMA, AND JAMAL AHMAD DARGHAM, (Senior Member, IEEE)
Faculty of Engineering, University Malaysia Sabah, Kota Kinabalu 88400, Malaysia
Corresponding author: Hoe Tung Yew (htyew@ums.edu.my)

This work was supported in part by the Ministry of Higher Education Malaysia, Fundamental Research Grant Scheme (FRGS) under Grant FRGS/1/2020/TK0/UMS/02/2; and in part by Universiti Malaysia Sabah.

ABSTRACT Fifth-generation (5G) networks consist of relatively smaller cells compared to legacy networks. Therefore, a user will take a shorter time toward the cell edge. This exposes the mobile station (MS) to frequent handovers, which are bottlenecks affecting the quality of service and user experience. In this study, we introduce a self-optimization method for three pivotal handover control parameters (HCPs): Threshold, Hysteresis and Time-To-Trigger. The proposed approach considers a holistic range of factors to determine the optimal values for these HCPs. These factors include the received power of reference signals (channel conditions), the speed and direction of the user (mobility profile), and the synchronization signal periodicity and handover procedure latency (representing system parameters). Through analytical deliberations, the study establishes a framework for achieving optimal HCPs to minimize the handovers, mitigate the ping-pong effects, reduce handover failures, and sustain a good throughput performance. Furthermore, considering the channel, user, and system parameters allowed cell-specific HCP optimization, enabling the implementation of this method with any of the measurement events outlined in the 3rd Generation Partnership Project (3GPP) release 16 for 5G. This study shows that concurrent self-optimization of Threshold, Hysteresis, and Time-To-Trigger can yield remarkable enhancement of handover performance.

INDEX TERMS Handover control parameters, self-optimization, handover threshold, handover hysteresis margin, handover time-to-trigger, 5G, small cell network.

NOMENCLATURE

$Thresh_{dynamic}$	Mobility-Aware Dynamic Self-Optimizing Signal Level Threshold.
$Hyst_{dynamic}$	Mobility-Aware Dynamic Self-Optimizing Hysteresis Margin.
$TTT_{dynamic}$	Mobility-Aware Dynamic Self-Optimizing Time-To-Trigger.
$Q_{rxlevmin}$	Minimum Reference Received Power.
ρ	Reference Signal Received Power.
p_{RS}	Effective Transmitted Power of the Reference Signal.
t	Time.
l	Distance Travelled by a Mobile Station.
d	3-D Separation Distance Between a Mobile Station and a Base Station.
d_0	Close-In Free-Space Reference Distance.
c	Speed of Light.
v	Speed of a Mobile Station.
ϕ	Direction of a Mobile Station.
f	Carrier Frequency.
n	Environmental Path Loss Factor.
χ_σ	Gaussian Noise Factor.
τ	RRC Signalling Delay During Handover (Handover Latency).

The associate editor coordinating the review of this manuscript and approving it for publication was Hassan Omar.

a	Handover Window Time Coefficient.
ϵ	Cell Type Factor.
x	Percentile of Hysteresis Margin.
ψ	Mobile Station Measurement Periodicity.
T	Running Time.
$k, \mathcal{K}$	Trajectory Number.
$\mathcal{T}$	Average Throughput.

I. INTRODUCTION

The fifth-generation cellular networks (5G) and beyond are designed to provide higher system capacity to meet the huge growth in global mobile data and demand for ubiquitous access to communication services. One of the effective approaches is to use smaller cells. The support of smaller cells has been a key feature of the 4G Long-Term Evolution-Advanced (LTE-A) systems, enabling flexible network deployment, improved cost-effectiveness, spectral efficiency, and user experience. In the 5G, system capacity has improved tremendously, due to the use of higher frequency bands (sub-6GHz to millimeter wave) and other enabling technologies, making 5G a type of small cell network [1]. Small cells have a coverage range from ten meters to several hundred meters; femtocells and picocells with less than 100m are deployed indoors, while microcells with coverage of a few hundred meters are typically deployed outdoors in rural and urban environments.

Nowadays, 5G outdoor base stations (BS) are being deployed in different cities around the world. However, optimization of handover control parameters (HCP) remains a challenging task for network operators. The 3rd Generation Partnership Project (3GPP) Radio Resource Control (RRC) protocol specifications for 5G, specifies mainly four HCPs, namely signal level Threshold, Hysteresis margin, Time-To-Trigger and Offsets [2]. Many optimization studies have been conducted mainly for Hysteresis and Time-To-Trigger [3]. Some authors have proposed using soft HCPs such as dwell time or distance [4], [5], [6], which has been implemented mostly for indoor access points, with dwell time accuracy concerns [7]. The current industrial practice of optimizing HCPs involves manual tuning of HCPs by leveraging human experience based on trials and sometimes using vendor-predefined values (fixed HCPs values). However, this manual approach is based on one-solution-fits-all scenarios without considering varying channel conditions and user mobility; hence, it is often suboptimal [8]. Moreover, the large number of small cells required for ubiquitous access in 5G and beyond makes the optimization problem more complex.

Two main factors that make the optimization of HCPs particularly challenging in small cell networks are user mobility and wireless channel conditions. Primarily, handover is a time-sensitive event, more so when user mobility is rapidly changing, e.g., from pedestrian to vehicular. Due to small coverage, the MS will take a shorter time to reach the cell-edge [9]. Therefore, for fast-moving MS, it is imperative to initiate and execute handover early and in a timely manner. This will ensure that handover is completed before the user exits the serving cell and therefore minimizing handover failures which affect the quality of service (QoS). In other situations, such as MS moving at pedestrian speed, it is preferred to delay the handover to avoid unnecessary or ping-pong handovers, which would render the usage of network resources inefficient. The ping-pong handovers cause signaling overhead, resulting in network congestion [10]. Therefore, using fixed HCP values could impose severe penalties in some situations, leading to sub-optimal overall performance.

Additionally, the optimization of HCPs is challenging due to rapid changes in the wireless channel conditions [11]. This is caused by radio frequency (RF) interference from neighbour cells, penetration loss and multipath effects, which are more prominent in urban environments. Therefore, in certain scenarios when MS is around the mid-cell region of the serving BS, it may suddenly receive a degraded channel quality. In this case, it might be more advantageous to impose higher HCP values that lead to a delay in handover and minimize the ping-pong effect. On the other hand, when the same HCP policy is applied at cell-edge, it could potentially lead to handover failures and, hence, poor quality of service.

Therefore, in this work, we propose self-optimization of three main HCPs, namely Threshold, Hysteresis and Time-To-Trigger by considering user speed and direction, channel conditions, and system parameters to determine the optimal values of HCPs for optimal handover performance. The proposed approach addresses the timing challenges of handovers (i.e., when to initiate handover) and the dynamic nature of the wireless channel (i.e., where to initiate handover). This is achieved by leveraging user mobility profile (speed and direction), channel condition through received signal power of the reference signal (RSRP), and system parameters such as the synchronization signal block (SSB) based measurement timing configuration (SMTC) and RRC delays during handover (handover latency)) in optimization of the HCPs. This makes the proposed method cell-specific, where the HCPs can be self-optimized based on the type of cell and its associated radio link and system configuration. This in turn should lead to optimal handover performance where handover frequency, ping-pong, and handover failures rates are minimized and hence improving the quality of service.

We propose three closed-form analytical expressions for each HCP where all input parameters to the proposed method are taken from current measurements performed by the MS. Each formula optimizes the HCP based on measurement from a specific cell, leading to two classifications of the self-optimization as either *serving cell-based HCP optimization* or *target cell-based HCP optimization*. To this end, we re-classified 3GPP handover measurement events as either serving cell-based (event A1, A2), target cell-based (A3, A4, B1 and A6), or both (A5 and B2). The proposed solution is in line with the current 3GPP standards, such as handover call flows, SMTC and 3GPP measurement events. Therefore,

the proposed solution would not require new standardization efforts.

The rest of the paper is organized as follows: Section II presents relevant works in literature and the contributions of this paper. Section III describes the handover procedure in 5G systems. Section IV presents a detailed description of the proposed method. Section V presents the proposed self-optimizations of three HCPs i.e., Threshold, Hysteresis, and Time-To-Trigger. In this section, mathematical formulations are presented. Section VI presents the performance evaluation of the proposed solution. This section presents simulation environment and parameters, handover key performance indicators (KPIs), numerical analysis of the self-optimizing HCPs, and the handover performance analysis of the proposed methodology in 5G networks. Finally, Section VII concludes this paper with recommendations for future works.

II. RELATED WORK AND CONTRIBUTIONS

A. RELATED WORK

Self-optimization in cellular networks attracted significant interest in research communities since the introduction of a Self-organizing network (SON) in 3GPP release 8 for LTE, which was enhanced for 5G systems in 3GPP release 17 in 2022 [12]. The SON functions play a key role in network automation by enabling self-configuration, self-optimization and self-healing using data collected from mobile stations (MS). Two SON functions responsible for HCP optimization are Load Balancing Optimization (LBO) and Mobility Robustness Optimization (MRO); they are designed for automatic configuration and update of HCPs to improve the handover performance. A conflict which is yet to be addressed. Authors in [13] provide an extensive survey on handover parameters self-optimization challenges in emerging networks and give insights on possible solutions. In recent years, several handover parameters optimization strategies have been proposed for 5G and beyond.

In [14], a fuzzy logic approach to adaptively optimize Hysteresis and Time-To-Trigger using MS speed, signal-to-interference-plus-noise ratio (SINR), and network load is introduced. Fuzzy logic is the simplest artificial intelligence method based on reasoning, which emulates human decision-making more closely, making it suitable for system control automation. However, fuzzy rules classify inputs into a limited set of linguistic variables leading to a rather "*discrete-time adaptive*" optimization that may not fully address continuously changing wireless environments. Additionally, increasing the number of fuzzy rules might increase delay in optimizing HCPs. Authors in [15] proposed a fuzzy-like method to adapt Hysteresis and Time-To-Trigger based on RSRP and user speed class. Three speed classes are used: *low*, *medium* and *high*. Like in fuzzy systems, this leads to a *discrete-time adaptive* optimization which is limited to the number of speed classes. Fewer classes lead to suboptimal HCPs. The main drawback of the fuzzy and fuzzy-like approach is that there is no standard to classify inputs, making the classification subjective that may not apply to a different scenario.

In [16], authors proposed a machine learning based approach to automatically optimize Threshold and Time-To-Trigger for inter-frequency handover based on RSRP, SINR, and handover success rate. This approach jointly optimizes mean values of handover key performance indicators (KPIs) as a function of expected values of HCPs using Genetic Algorithm and XBoost machine learning model, where training data sampling is based on important ranges of Thresholds and Time-To-Trigger, a technique which has shown faster convergence time compared to regular sampling. However, one of the main challenges of the joint HCP-KPI optimization is handover failures must occur before the algorithm adjusts HCPs to optimal values, leading to slow response and late optimization. Additionally, parameters related to user mobility are not clearly addressed despite having a direct impact on handover performance. To overcome the weakness of previous studies, authors in [17] proposed online Q-learning-based optimization of the Hysteresis and Time-To-Trigger based on RSRP predictions using Karman filter. The Karman filter takes current RSRP measurements as input and it estimates the posteriori of the RSRP which is then used in the reinforcement learning module to adaptively choose the optimal Hysteresis and Time-To-Trigger values. Although the online reinforcement learning took into accounts RSRP and user mobility, the accuracy of this approach is limited to the prediction accuracy of future RSRP measurements. In high interference and highly mobile scenarios, prediction becomes less accurate, leading to suboptimal handover performance. Moreover, for denser network of 5G small cells, the Q-learning might increase handover delay due to the query of larger Q-table [10]. Some authors have proposed using network slicing to reduce action space [18], [19], [20]. Nonetheless, machine learning techniques require sufficient and reliable data for training purposes, where the accuracy and reliability of the model is based on the quality (representativeness) and size of the training data. An extensive survey on machine learning solutions to handover parameters optimization is presented in [21]. In summary, existing machine learning approaches for HCP optimization use subjective and limited training data, which may not be sufficient to train robust models. Additionally, service providers may not afford to try larger data sets on a live network due to the inherent risk of performance loss during the learning processes [8].

Other researchers followed a different approach compared to the previously discussed literature by proposing new HCP optimization methods using an analytical approach. An initial attempt at an analytical approach to optimize the handover process was introduced in [22]. The authors derive probability models for cell coverage and handover KPIs as functions of Time-To-Trigger, user density and speed. A similar approach is presented in [23], where the probability models were analyzed in both fading and no fading scenarios. The probability

approach gives insight into a better HCP setting for a given scenario, hence providing guidance for actual network planning. This minimizes the time-consuming trial-based manual tunning. However, it does not directly and automatically optimize the HCP; therefore, it still requires manual intervention by operators to update to the optimal HCP setting upon numerical simulation of the probability models. To overcome this, authors in [24] introduced analytical expressions to acquire Hysteresis optimal range for a particular user speed and predefined Time-To-Trigger value. The analytical models consider both channel and system parameters and utilize a generic fading model at the cell-edge where too-late, too-early or ping-pong handovers are anticipated. The optimal Hysteresis value is selected from the acquired optimal range; this has improved performance compared to selecting from a default 3GPP range. However, it is not clear how the optimal value is selected from the optimal range. With a large range, choosing an optimal value becomes challenging. Moreover, only one HCP was optimized in this study. Additionally, the approach requires operators to obtain optimal Hysteresis range for each user speed and Time-To-Trigger, which is impractical in dynamic environments. In addressing the issue of selecting an optimal value from the range, authors in [25] used the ratio of serving and target cell RSRPs to determine the optimal Hysteresis value bounded by the default 3GPP range in LTE-A. They used a regression model to determine optimal Time-To-Trigger based on Hysteresis and user speed. The regression model is generated based on a set of 10 values of Hysteresis, Time-To-Trigger and user speed with intervals of 0.5 dB, 160 ms, and 15 km/h, respectively, using 3GPP default range. The approach has outperformed the classical fixed HCP approach. In [26], the authors presented a regression model that correlates Hysteresis and Event A3 offset with inter-site distance and user direction (angle of MS movement). The regression model is generated using 3GPP default range for Hysteresis and Event A3 offset with the interval of 5 dB, where a model with better goodness-of-fit was achieved with a fourth-degree polynomial. The model is then used to obtain optimal Hysteresis and Event A3 offset at the current inter-site distance and user direction (angle of MS movement). One of the limitations of this study is with higher-degree polynomials, the amount of computation increases. Additionally, in both studies, the regression models are obtained from limited discrete data set from 3GPP default set; low granularity of the data set may result to a sub-optimal regression model. Moreover, the regression models did not include channel and system-related parameters such as signal quality, measurement timing and receiver sensitivity, which affects measurements directly. This lack of direct correlation to system behaviours can degrade the handover performance.

To the best of the authors' knowledge, no study exists in the literature that proposes the optimization of all three main HCPs: Threshold, Hysteresis, and Time-To-Trigger. Moreover, existing works deal with optimization in one handover measurement event of choice. Optimization performed for a particular measurement event may not be applicable to another. In addition, in some studies, optimization is based on previous performance history therefore may not be suitable in live network due to rapidly changing network conditions and time sensitive nature of handovers in 5G small cells. This motivates a mobility-aware dynamic self-optimization of key HCPs based on the current channel conditions, user mobility, and system parameters such that a low handover rate and high throughput performance can be achieved.

B. CONTRIBUTION

The contributions and novelties of this paper are summarized as follows:

1) It is the first study to investigate the impact of user mobility, channel condition and system timing configuration on three key HCPs namely Threshold, Hysteresis and Time-To-Trigger: in both relative and absolute handover measurement strategies re-classified as serving cell-based optimization (event A1, A2), target cell-based optimization (A3, A4, B1 and A6), or both (A5 and B2). The analysis showed that there exists correlation for each of the three key HCPs with user mobility, channel condition and system parameters. Furthermore, the analysis reveals that the optimal values are not constrained to the cell-edge where handover is mostly anticipated. It is possible to obtain optimal combination of HCP values in any location within cell, this is useful in maintaining good handover performance during severe signal fluctuations.
2) We have formulated the analytical closed-form expression to dynamically and automatically determine the optimal values of Threshold, Hysteresis and Time-To-Trigger based on current measurement of user mobility (speed and direction), channel condition (RSRP), and system timing configuration (measurement timing configuration based on SMTC and RRC delays during handover). The measurement of RSRP, SMTC, and RRC signalling delay is cell-specific. Therefore, the self-optimization is cell-specific, allowing this method to be applied with any handover measurements event specified in 3GPP TS 38.331. The analytical models, therefore, can be applied to optimize HCP in either inter-RAT (homogeneous network) or intra-RAT (heterogeneous network).
3) The proposed model takes input directly from current measurement performed by MS. The proposed solution does not require new standardization efforts. This allows for direct implementation in real networks.

III. HANDOVER PROCEDURE IN 5G SYSTEMS

Handover enables user's session transfer between cells for better service continuity. In cellular networks, handover is based on measurement report (MR) from MS to BS. The MS periodically measure the RSRP of available BSs, and eventually or periodically sends MRs to the serving BS, where

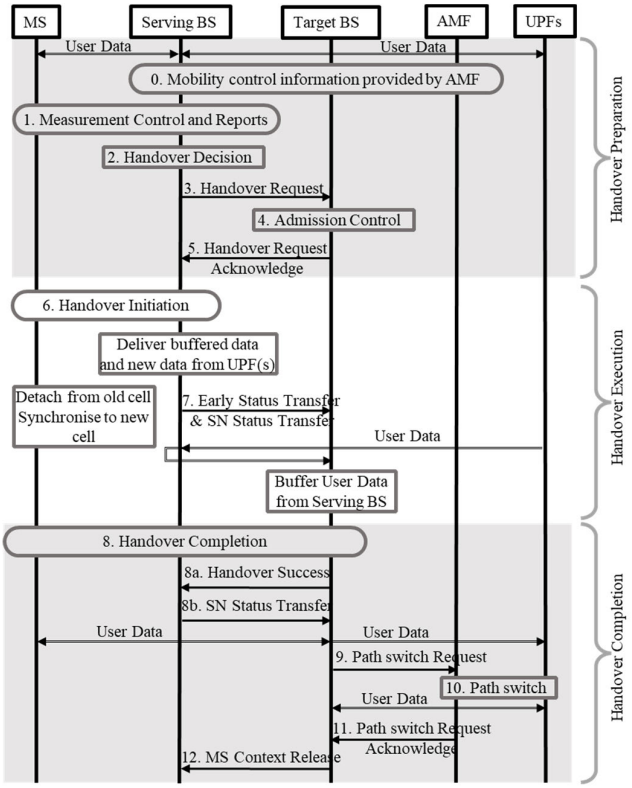

FIGURE 1. Handover procedure in 5G systems.

handover decision is performed to determine the best target cell. Fig. 1 depicts the basic handover scenario in 5G systems where neither the Access and Mobility Management Function (AMF) nor the User Plane Function (UPF) changes [27]. The handover process in 5G systems is divided into three phases namely handover preparation, handover execution and handover completion, comprised of mainly 12 steps [27].

A. HANDOVER PREPARATION PHASE

It is comprised of five steps. *Step 1*: The serving BS configures the MS measurement procedures, and the MS sends MRs to serving BS according to measurement configurations. *Step 2*: The serving BS perform handover decision to determine the best target based on received MRs and radio resource management (RRM) information. *Step 3*: The serving BS issues a Handover Request message to the target BS passing a transparent RRC container with necessary information to prepare the handover at the target BS. *Step 4*: The target BS performs Admission Control. *Step 5*: The target BS prepares the handover with Layer 1 and Layer 2 and sends the Handover Request Acknowledge to the serving BS including transparent container as RRC message to perform the handover (Handover Command).

B. HANDOVER EXECUTION PHASE

Starts off at *Steps 6* where the target BS triggers the Uu interface handover by sending an RRC Reconfiguration message

TABLE 1. Handover measurement events.

Handover Event (Measurement Report Criteria)	Condition	
Event A1	Serving BS becomes better than threshold. $RSRPserving > RSRPthresh + Hyst$	Absolute Measurement
Event A2	Serving BS becomes worse than threshold. $RSRPserving < RSRPthresh - Hyst$	Absolute Measurement
Event A3	Target BS becomes offset better than primary Serving BS. $RSRPtarget > RSRPserving + Hyst + Offc$	Relative Measurement
Event A4 / Event B1 for inter-RAT	Target BS becomes better than threshold. $RSRPtarget > RSRPthresh + Hyst$	Absolute Measurement
Event A5 / Event B2 for inter-RAT	Serving BS becomes worse than first threshold and target BS becomes better than second threshold. $RSRPserving < RSRPthresh1 - Hyst$, $RSRPtarget > RSRPthresh2 + Hyst$	Absolute Measurement
Event A6	Target BS becomes offset better than secondary Serving BS. $RSRPtarget > RSRPserving + Hyst + Offc$	Relative Measurement

to the MS. The message contains information required to access the target BS such as target cell ID, new RRC connection and scheduling identifier C-RNTI (Cell Radio Network Temporary Identifier), security algorithm identifiers, random access channel (RACH) resources and its association. *Step 7*: The serving BS sends the Early Status Transfer message for Dual Active Protocol Stack (DAPS) handovers (when Data Radio Bearer (DRB) is configured with DAPS), also known as make-before-break or soft-handover; where the serving BS does not stop transmitting downlink packets until it receives the Handover Success message from the target BS. Meanwhile, for DRBs not configured with DAPS, the serving BS sends the SN Status Transfer message to the target BS.

C. HANDOVER COMPLETION PHASE

Starts off at *Step 8* where the MS synchronizes to the target BS and completes the RRC handover procedure by sending RRC Reconfiguration Complete message to the target BS. In the case of DAPS handover, the MS does not detach from the serving BS upon receiving the RRC Reconfiguration message except until the target BS sends the Handover Success message to the serving BS to inform that the MS has successfully accessed the target cell. Finally, the serving BS sends the SN Status Transfer message where normal data forwarding begins. *Step 9:* The target BS sends a Path Switch Request message to AMF to trigger the 5G core (5GC) to switch the downlink data path towards the target BS and to establish a control plane (C-Plane) interface instance towards the target BS. *Step 10:* The 5GC switches the downlink data path towards the target BS, and the UPF sends "end marker" packets on the old path to release any user plane (U-Plane) resources. *Step 11:* The AMF confirms the Path Switch Request message with the Path Switch Request Acknowledge message. *Step 12:* Upon reception of the Path Switch Request Acknowledge message from the AMF, the target BS sends the MS Context Release to inform the serving BS about the success of the handover.

Step 1 and *Step 2* have gained more attention in the research community, especially on the optimization of HCPs and handover decision making algorithms. The handover measurement checks whether handover should be performed

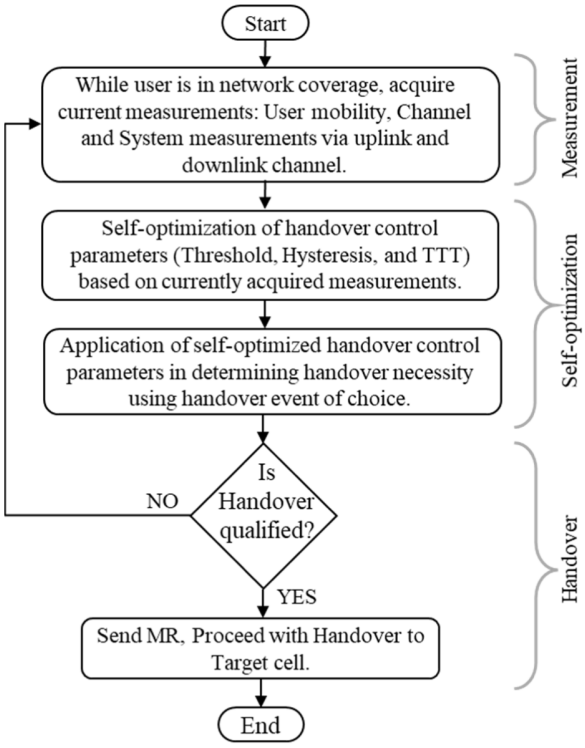

FIGURE 2. Block diagram of the proposed methodology.

based on certain conditions of the downlink channel of either the serving cell, target cell or both. The HCPs are combined with downlink channel measurement items such as RSRP to form handover measurement events condition to determine when handover is necessary and report the event to the serving BS through MRs. The 3GPP RRC Protocol for 5G has proposed six set of handover measurement events conditions [2], as shown in Table 1.

The handover events can be classified based on measurement strategy as either *Relative Measurement* where serving cell and target cell measurements are compared directly, or *Absolute Measurement* strategy where serving cell or target cell measurements are compared against threshold.

IV. DESCRIPTION OF METHODOLOGY

This section describes the methodology to optimize handover for 5G and beyond networks. The methodology can be divided into three stages, as shown in Fig 2.

The *first stage* consists of the collection of measurements that are user, channel and system-related. User-related measurements include mobility profile such as user speed, direction and estimated distance from BS. These can be assisted by high-precision location and speed sensors. Channel-related measurements include RSRP and SINR. System-related measurements include transmit power, bandwidth, frequency, and SMTC periodicity which is used to configure MS measurement periodicity. These measurements are communicated back and forth between MS and BS via uplink and downlink channels. In the downlink channel, the BS sends the systems

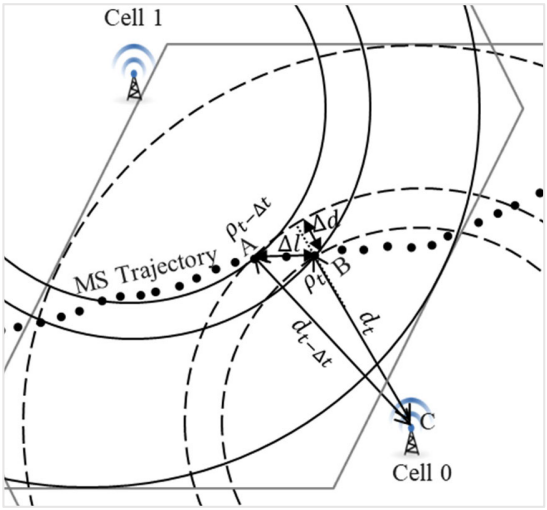

FIGURE 3. Mobile Station (MS) traversing in a network cell.

information. In the uplink channel, the MS typically compiles channel and device measurements into a measurement report to send to serving BS based on certain periodicity for periodic measurement or based on event for event-based measurement. The currently acquired measurements are then used to optimize the HCPs.

The *second stage* of the methodology is the self-optimization stage, where the currently acquired measurements are used to obtain optimal values of Threshold, Hysteresis, and Time-To-Trigger. The optimal HCP values are then used in the handover event of choice to facilitate optimal handover performance. The proposed closed-form expression for self-optimization of HCPs is presented in section V.

The *third stage* of the methodology is the application of optimized HCPs in a handover process. The optimal HCP values are applied to determine the necessity of handover using handover event of choice. Handover is qualified when a handover event qualifies, and Time-To-Trigger expires. Once the handover qualifies, the system proceeds with handover procedures to the best target cell. The best target cell is selected from candidate cells using any selection and ranking method of choice.

V. SELF-OPTIMIZATION OF HANDOVER CONTROL PARAMETERS

This section describes the approach to optimize three main HCPs for 5G and beyond networks. We propose a mobility-aware dynamic self-optimizing HCPs based on a user's mobility profile, channel measurement, and system behavior.

Consider a Mobile Station (MS) moving from position A to B in a cell, travelling a small distance Δl along the trajectory for a small duration Δt, as shown in Fig. 3. Let ρ_t and $\rho_{t-\Delta t}$ be RSRP of cell i measured by the MS at time t (point B) and time $t - \Delta t$ (point A), respectively, where d_t and $d_{t-\Delta t}$ are the corresponding separation distance from MS to BS (d) at

time t and time $t - \Delta t$, respectively, forming a small region of size Δd.

The relationship between ρ and d is given by channel propagation models. Various propagation models are presented and discussed in [28]. Modelling of channel propagation can be categorized into two types: close-in model where a physical anchor that captures the path loss near the transmitter is used. Another type is the floating-intercept model, which has no physical reference, but merely fits the best line to the measured data (via a least-square regression) to create a floating-intercept linear equation model. In this paper, the close-in model is used because of its standard usage, frequency dependence, and the ease by which measurements across different bands and scenarios can be compared [29]. The propagation path loss over frequency and distance, in dB, using close-in model is shown in (1).

$$\mathrm{PL}\,(f\,,d) = \mathrm{FSPL}\,(f\,,d_0) + 10n\log_{10}\left(\frac{d}{d_0}\right) + \chi_\sigma\,, d \geq d_0 \tag{1}$$

where $\mathrm{FSPL}\,(f\,,d_0)$ is the close-in free space path loss in dB given by $10\log_{10}\left(\frac{4\pi f d_0}{c}\right)^2$ and is a function of carrier frequency f, d_0 is the close-in free-space reference distance and c is the speed of light, n denotes the best fit minimum mean square error path loss factor over all measurements from a particular measurement campaign. χ_σ is a zero-mean Gaussian random variable with a standard deviation σ in dB, also known as the shadow fading factor, representing large-scale signal fluctuations resulting from shadowing by large obstructions in the wireless channel. The propagation path loss (PL) is the difference between transmitted power and received power; it is given as $\mathrm{PL} = p_{\mathrm{RS}} - \rho$ in decibel scale, where p_{RS} is the effective transmitted power of the reference signal and ρ is RSRP. We use reference distance, $d_0 = 1$ m, which is typical for both line-of-sight (LOS) and non-line-of-sight (NLOS) environments [29]. Therefore, ρ in dBm relates to the 3-D separation distance d according to (2).

$$\rho = p_{RS} - 10\log_{10}\left[\left(\frac{4\pi f}{c}\right)^2 (d)^n\right] - \chi_\sigma \tag{2}$$

From (2), d_t and $d_{t-\Delta t}$ can be expressed as shown in (3) and (4) respectively.

$$d_t = 10^{\left(\frac{p_{RS} - \rho_t - 20\log_{10}\left(\frac{4\pi f}{c}\right) - \chi_{\sigma,t}}{10n}\right)} \tag{3}$$

$$d_{t-\Delta t} = 10^{\left(\frac{p_{RS} - \rho_{t-\Delta t} - 20\log_{10}\left(\frac{4\pi f}{c}\right) - \chi_{\sigma,t-\Delta t}}{10n}\right)} \tag{4}$$

Consider the small displacement Δd in Cell 0 as shown in Fig 3, for a much smaller time difference Δt:

$$d_{t-\Delta t} = d_t + \Delta d \tag{5}$$

Substitute (4) and (5) into (3).

$$10^{\left(\frac{p_{RS} - \rho_{t-\Delta t} - 20\log_{10}\left(\frac{4\pi f}{c}\right) - \chi_{\sigma,t-\Delta t}}{10n}\right)}$$

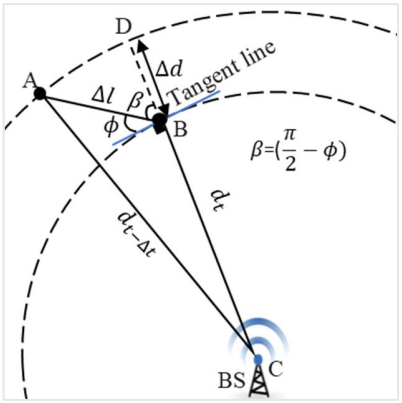

FIGURE 4. Illustration of MS tangent angle ϕ formed by MS trajectory segment Δl and Tangent line at current MS location.

$$= 10^{\left(\frac{p_{RS} - \rho_t - 20\log_{10}\left(\frac{4\pi f}{c}\right) - \chi_{\sigma,t}}{10n}\right)} + \Delta d$$

Let $\mathrm{K} = 10^{\left(\frac{p_{RS} - 20\log_{10}\left(\frac{4\pi f}{c}\right)}{10n}\right)}$, therefore,

$$K * 10^{-\left(\frac{\rho_{t-\Delta t} + \chi_{\sigma,t-\Delta t}}{10n}\right)} = K * 10^{-\left(\frac{\rho_t + \chi_{\sigma,t}}{10n}\right)} + \Delta d \tag{6}$$

Multiply by $10^{\left(\frac{\rho_t + \chi_{\sigma,t}}{10n}\right)}$ on both sides of (6), we obtain Δd given as:

$$\Delta d = \frac{K}{10^{\left(\frac{\rho_t + \chi_{\sigma,t}}{10n}\right)}}\left(10^{\left(\frac{\rho_t + \chi_{\sigma,t} - \rho_{t-\Delta t} - \chi_{\sigma,t-\Delta t}}{10n}\right)} - 1\right) \tag{7}$$

By substituting K into (7), the term $\frac{K}{10^{\left(\frac{\rho_t + \chi_{\sigma,t}}{10n}\right)}}$ becomes equal $10^{\left(\frac{p_{RS} - 20\log_{10}\left(\frac{4\pi f}{c}\right) - \rho_t - \chi_{\sigma,t}}{10n}\right)}$ which is d_t as given in (3). Therefore,

$$\Delta d = d_t\left(10^{\left(\frac{\rho_t - \rho_{t-\Delta t} + (\chi_{\sigma,t} - \chi_{\sigma,t-\Delta t})}{10n}\right)} - 1\right) \tag{8}$$

We assume that the difference of the shadow fading factors at a smaller time difference Δt is insignificant i.e., $\chi_{\sigma,t} - \chi_{\sigma,t-\Delta t} \approx 0$. Therefore: -

$$\Delta d = d_t\left(10^{\left(\frac{\rho_t - \rho_{t-\Delta t}}{10n}\right)} - 1\right) \tag{9}$$

where d_t is the separation distance between BS and MS at current time t, and $\rho_t - \rho_{t-\Delta t}$ is the difference between the RSRP at current MS location at time t and previous MS location with time difference Δt. Equation (9) is for all three cases of MS directivities:

Case I: When the MS moves for a duration Δt such that $\rho_t = \rho_{t-\Delta t}$(travels along the line of equal received power or field strength), then the Δd will be zero ($\Delta d = 0$).

Case II: When the MS moves for a duration Δt such that $\rho_t > \rho_{t-\Delta t}$(travels closer to the cell center), then the Δd will be positive ($\Delta d > 0$).

Case III: When the MS moves for a duration Δt such that $\rho_t < \rho_{t-\Delta t}$(travels away from the cell center), the Δd will be negative ($\Delta d < 0$).

To obtain the relationship between RSRP difference in time duration Δt and user mobility within a particular cell, we derived Δd in terms of user speed and direction.

In Fig. 4, it is shown that when the MS is at location $B(x_{MS,t}, y_{MS,t})$, at time t, it has a tangent line perpendicular to a line (or plane) connecting the BS and MS current location B.

Let $m_{\Gamma,t}$ and $m_{BS,t}$ be slope of the tangent line and slope of the line connecting BS and MS at location B, respectively. Due to the perpendicular property of the two lines; $m_{\Gamma,t} * m_{BS,t} = -1$. The BSs are static; therefore, their position is fixed. We assume that the Cell i^{th} BS is positioned at $(x_{BS,i}, y_{BS,i})$. Therefore, the slope of the tangent line is given by $m_{\Gamma,t} = -\frac{1}{m_{BS,t}} = -(x_{BS,i} - x_{MS,t})/(y_{BS,i} - y_{MS,t})$. Given the location $A(x_{MS,t-\Delta t}, y_{MS,t-\Delta t})$, the slope of the MS route segment Δl, is given by $m_{\Delta l,\Delta t} = (y_{MS,t} - y_{MS,t-\Delta t})/(x_{MS,t} - x_{MS,t-\Delta t})$. The MS tangent angle ϕ at time t is therefore given by (10).

$$\phi_t = \arctan\left(\frac{m_{\Delta l,\Delta t} - m_{\Gamma,t}}{1 + m_{\Delta l,\Delta t} * m_{\Gamma,t}}\right) \tag{10}$$

By using trigonometric rule:

$$\mathrm{Cos}\,(\pi/2 - \phi_t) \approx \Delta d/\Delta l = \mathrm{Sin}\phi_t \tag{11}$$

Since Δt is the time taken to travel Δl, we consider Δt is much smaller in order of MS measurement periodicity, and such that the change in MS speed on Δl is negligible. Therefore, the average MS speed at $t - \Delta t$ to t becomes approximately equals to MS speed at time t i.e., v_t. Therefore $\Delta l = v_t \Delta t$. By substituting Δl into (11), Δd can then be expressed using user speed (v_t) and direction (ϕ_t) as shown in (12).

$$\Delta d = v_t \Delta t \mathrm{Sin}\phi_t \tag{12}$$

It is important to note that, $\Delta d = 0$ when $\phi_t = 0$. This occurs when the MS moves along the tangent line such that $m_{\Delta l,\Delta t} = m_{T,t}$. For a small duration Δt, this resemble **Case I** of MS directivity where $\rho_t = \rho_{t-\Delta t}$. Similarly, $\Delta d > 0$ when $\phi_t > 0$ i.e., $m_{\Delta l,\Delta t} > m_{\Gamma,t}$; and $\Delta d < 0$ when $\phi_t < 0$ i.e., $m_{\Delta l,\Delta t} < m_{\Gamma,t}$; which resemble **Case II** and **Case III**, respectively. Without losing generality, we consider only magnitude of the displacement by taking $|\phi_t|$. Solving (9) and (12), yields (13). This is the guiding equation in our optimization.

$$\rho_t - \rho_{t-\Delta t} = 10n\log_{10}\left(\frac{v_t \Delta t \mathrm{Sin}\,|\phi_t|}{d_t} + 1\right) \tag{13}$$

Equation (13) gives an analytical model that relates the receive power difference ($\rho_t - \rho_{t-\Delta t}$), time difference Δt, path loss factor n, user speed v_t and direction ϕ_t, and separation distance d_t from current user location to Cell's BS. The path loss factor n is the environmental parameter ranging from 2.1 to 3.5 for urban microcell [30]. We use the guiding equation in (13) to obtain self-optimizing handover control parameters (HCPs) formulas.

TABLE 2. Handover events classification based on cell specific HCP optimization.

	Absolute Handover Measurement Strategy	Relative Handover Measurement Strategy
Serving Cell Based HCP Optimization	A1, A2	–
Target Cell Based HCP Optimization	A4, B1	A3, A6
Serving and Target Cell Based HCP Optimization	A5, B2	–

A. SELF-OPTIMIZING THRESHOLD

The self-optimizing Threshold, also known as mobility-aware dynamic Threshold ($Thresh_{dynamic}$) is obtained by offsetting the minimum reference received power by $\Delta\rho$. The minimum reference received power of a certain cell is known to the MS through System Information Base (SIB) as minimum required received level ($Q_{rxlevmin}$) [31]. Therefore, $Thresh_{dynamic}$ can be derived as follows:

$$Thresh_{dynamic} = \mathrm{Q_{rxlevmin}} + \Delta\rho \tag{14}$$

The $\Delta\rho$ is derived from (13),

$$\Delta\rho = \rho_t - \rho_{t-\Delta t}$$
$$\Delta\rho = 10n\log_{10}\left(\frac{v_t \Delta t \mathrm{Sin}\,|\phi_t|}{d_t} + 1\right) \tag{15}$$

The MS speed v_t, tangent angle ϕ_t and separation distance are measured by the MS at given time t. The Δt is a time control parameter, it is selected in such a manner that will offer enough time for MS at a particular speed to complete handover. Therefore, the Δt must be higher than the RRC signalling delay during handover procedures (handover latency) and time-to-trigger combined. This is to ensure that optimizations are constrained within system properties. For instance, for a given a system with handover latency τ, Δt can be a multiple of handover latency i.e., $\Delta t = a\tau$. Equation (14) becomes:

$$Thresh_{dynamic} = Q_{rxlevmin} + 10n\log_{10}\left(\frac{v_t a\tau \mathrm{Sin}\,|\phi_t|}{d_t} + 1\right) \tag{16}$$

where $Q_{rxlevmin}$ is minimum reference received power, n is path loss factor, v_t is MS speed at time t, ϕ_t is MS direction angle at time t, d_t is MS to BS separation distance at time t, τ is RRC signalling delay during handover and a is handover window time coefficient.

The handover window time coefficient a offers some configurability and scalability since different system may offer different time configurations. We have considered $a \geq 2$, for handover window that accommodates at least *inbound* and *outbound* handover at each time. A smaller or larger a increases the risk of a *too-late* or *too-early* handover respectively. Therefore, for a particular MS speed, the cell

minimum received level $Q_{rxlevmin}$ is offset by a region that can accommodate both *inbound* and *outbound* handovers, given that *inbound* and *outbound* handovers exhibit approximately equal latency; otherwise, a maximum of the two is used.

Parameters $Q_{rxlevmin}$, τ, and d_t are cell-dependent. Since (16) is based on serving cell, we extend our method further by considering cell type (target cell or serving cell) and the handover measurement strategy involved (either relative or absolute). For clarity, we classified handover events into *serving cell-based HCP optimization*, *target cell-based HCP optimization*, and both *serving and target cell-based HCP optimization* as shown in Table 2.

In the *serving cell-based HCP optimization*, the HCPs are obtained using parameters related to serving cell. Events that fall into this category are A1 and A2; both are based on absolute measurement strategy. For the *target cell-based HCP optimization*, the HCPs uses parameters from target cell, and it includes A4 and B1 both use absolute measurement strategy; and A3 and A6 which use relative measurement strategy. Lastly, *serving and target cell-based HCP optimization*, the HCPs use parameters related to both serving and target cells and it includes A5 and B2 which use absolute measurement strategy.

To further understand the serving and target cell specific optimization, consider the guiding equation in (13). From this equation, the power margin $(\rho_t - \rho_{t-\Delta t})$ increases when user speed v_t increases and vice versa (assuming other factors remain constant). This power margin is added to $Q_{rxlevmin}$ for the case of $Thresh_{dynamic}$ in (16). Therefore, the $Thresh_{dynamic}$ will increase as user speed v_t increases and vice versa.

This will be advantageous for the *serving cell-based HCP optimization*, because by increasing the serving threshold and margin for a fast-moving user will allow handover to be performed before MS exits serving cell therefore minimizing *too-late* handovers and handover failures. Similarly, decreasing the serving threshold and margin for a slow-moving user will minimize *too-early* handovers and hence minimize unnecessary handovers and ping pong effect.

However, it will be disadvantageous for the *target cell-based HCP optimization*, as increasing the targets threshold and margin for a fast-moving user will result to MS exiting serving cell before handover is performed, therefore maximizing *too-late* handovers and handover failures. Decreasing the target threshold and margin for a slow-moving user will maximize *too-early* handovers and hence, unnecessary handovers and the ping-pong effect.

To address this disadvantage, we applied multiplicative inverse to the *target cell-based HCP optimization* case to reverse the behaviour. Therefore, increasing user speed v_t will result in a decrease in the target threshold and margin, and vice versa.

Let ϵ be cell type factor; $\epsilon = 1$ for *serving cell-based HCP optimization* and $\epsilon = -1$ for *target cell-based HCP optimization*. Therefore, the self-optimizing Threshold is given by (17).

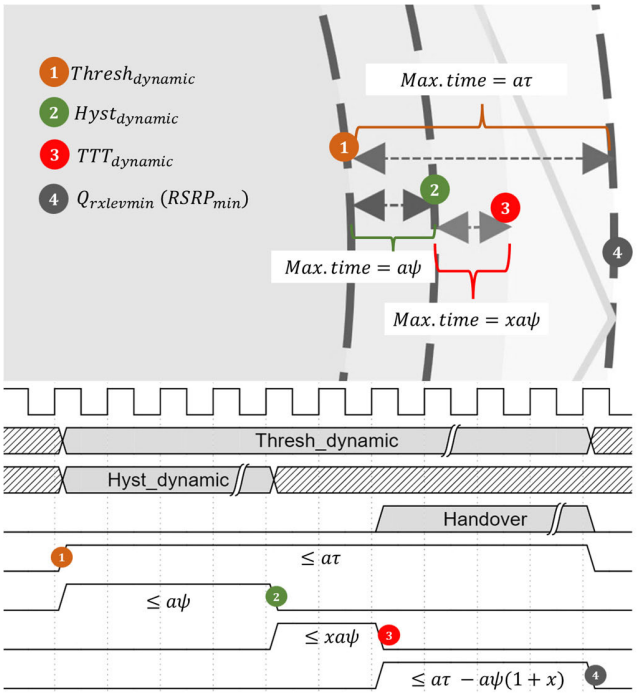

FIGURE 5. Illustration of the timing scenario in serving cell.

$$Thresh_{dynamic} = \mathrm{Q_{rxlevmin}} + \left(10n\log_{10}\left(\frac{v_t a\tau \mathrm{Sin}\,|\phi_t|}{d_t} + 1\right)\right)^{\epsilon} \quad (17)$$

By considering cell type (serving, target) dependency on HCP optimization, it makes this optimization solution applicable to both inter-RAT and intra-RAT handovers, as measurement from different RAT can lead to different system response.

B. SELF-OPTIMIZING HYSTERESIS

The self-optimizing Hysteresis margin, also known as mobility-aware dynamic Hysteresis ($Hyst_{dynamic}$) is derived from (13) by considering parameter Δt as the measurement periodicity at the MS. The measurement periodicity at MS is based on SMTC. In 5G systems, SMTC periodicity are in the range of 5, 10, 20, 40, 80 or 160 ms [32]. Let ψ be MS measurement periodicity; therefore $\Delta t = a\psi$, where a is a handover window time coefficient as established in subsection *A,* it is important to note that, $a\psi$ is much less than the maximum handover window $a\tau$ i.e., $a\psi \ll a\tau$. The self-optimizing Hysteresis is given by (18).

$$Hyst_{dynamic} = 10n\log_{10}\left(\frac{v_t a\psi \mathrm{Sin}\,|\phi_t|}{d_t} + 1\right) \quad (18)$$

By considering cell type as established in subsection A, the self-optimizing Hysteresis $Hyst_{dynamic}$ is given by (19), where cell type factor $\epsilon = 1$ for *serving cell-based HCP optimization* and $\epsilon = -1$ (multiplicative inverse) for *target*

cell-based HCP optimization.

$$Hyst_{dynamic} = \left(10n\log_{10}\left(\frac{v_t a\psi \,\mathrm{Sin}\,|\phi_t|}{d_t} + 1\right)\right)^{\epsilon} \quad (19)$$

C. SELF-OPTIMIZING TIME-TO-TRIGGER

The self-optimizing Time-To-Trigger, also known as mobility-aware dynamic Time-To-Trigger ($TTT_{dynamic}$) is derived from (13) by making the Δt the subject of the formular. We consider $\rho_t - \rho_{t-\Delta t}$ as a fraction x of a hysteresis margin $Hyst_{dynamic}$. The $TTT_{dynamic}$ is estimated as follows:

$$TTT_{dynamic} = \frac{d_t}{v_t \mathrm{Sin}\,|\phi_t|}\left(10^{\left(\frac{x(\mathrm{Hyst_{dynamic}})}{10n}\right)} - 1\right) \quad (20)$$

By substituting $Hyst_{dynamic}$ in (20) with (18), we get

$$\begin{aligned} TTT_{dynamic} &= \frac{d_t}{v_t \mathrm{Sin}\,|\phi_t|}\left(10^{\left(x\log_{10}\left(\frac{v_t a\psi \mathrm{Sin}|\phi_t|+d_t}{d_t}\right)\right)} - 1\right) \\ TTT_{dynamic} &= \frac{d_t}{v_t \mathrm{Sin}\,|\phi_t|}\left(\left(\frac{v_t a\psi \,\mathrm{Sin}\,|\phi_t| + d_t}{d_t}\right)^{x} - 1\right) \end{aligned} \quad (21)$$

Consider Fig. 5, when $x = 1$ i.e., 100 percentile of hysteresis margin, then maximum $TTT_{dynamic}$ i.e., $x(a\psi)$ becomes equal to the maximum time taken by the MS to cross the maximum hysteresis margin ($a\psi$) i.e., $x(a\psi) = a\psi$. The $x(a\psi)$ becomes less than $a\psi$ when $x < 1$ and vice-versa. The guiding principle is that the sum of the $a\psi$ and $x(a\psi)$ should be much less than maximum handover window $a\tau$ as shown in Fig. 5. Smaller value of x is desirable to ensure enough time is reserved for handover to complete before MS exits cell's $Q_{rxlevmin}$.

To minimize mathematical complexity, we assume x is 0.5 (50 percentile), which means the maximum time that MS could take as Time-To-Trigger is half the maximum time incurred on the Hysteresis margin. In this case, at maximum, the Hysteresis margin and Time-To-Trigger will consume $\psi(1+x)/\tau$ *100 percentile of the maximum handover window $a\tau$. Suppose a system with handover latency $\tau = 1$ s and MS measurement period of $\psi = 160$ ms, if $x = 0.5$, Hysteresis margin and Time-To-Trigger will at maximum occupy 24% of maximum time window $a\tau$, while reserving 76% for handover procedures. Since $a \geq 2$, 76% of $a\tau$ is higher than the handover latency τ. With this assumption, the self-optimizing Time-To-Trigger ($TTT_{dynamic}$) can be computed by (22).

$$TTT_{dynamic} = \frac{d_t}{v_t Sin\,|\phi_t|}\left(\sqrt{\frac{v_t a\psi \,Sin\,|\phi_t| + d_t}{d_t}} - 1\right) \quad (22)$$

By considering cell type as established in subsection A, the self-optimizing Time-To-Trigger ($TTT_{dynamic}$) is given by (23), where the cell type factor c is introduced, where $\epsilon = 1$ for *serving cell-based HCP optimization* and $\epsilon = -1$ (multiplicative inverse) for *target cell-based HCP optimization.*

$$TTT_{dynamic} = \left(\frac{d_t}{v_t Sin\,|\phi_t|}\left(\sqrt{\frac{v_t a\psi \,Sin\,|\phi_t| + d_t}{d_t}} - 1\right)\right)^{\epsilon} \quad (23)$$

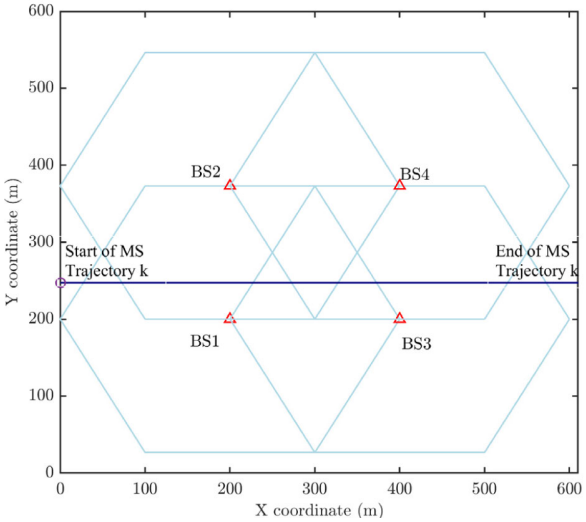

FIGURE 6. Deployment of 5G cells.

TABLE 3. System and environmental parameters.

Parameters	Value
Simulation environment size	600m x 600m
Number of routes/trajectories	200
Number of BS	4
Cell radius	200 m
BS max. transmit power	38 dBm
Carrier frequency	3.5 GHz
Numerology	1
Channel bandwidth	100 MHz
Sub-carrier spacing	30 KHz
Physical resource block	273 PRBs
Modulation scheme	AMC
MIMO scheme	2x2
Minimum received power	-101.5 dBm
MS measurement periodicity	160 ms
Handover time window	1s
Shadow fading	8 dB
Path loss exponent	3.5
MS Noise figure	7 dB
Thermal Noise Power Density	-174 dBm/Hz
MS speed	0 – 120km/h
Mobility model	Directional mobility

VI. PERFORMANCE EVALUATION

This section evaluates the proposed self-optimizing HCPs. The effect of various parameters on the proposed self-optimizing $Thresh_{dynamic}$, $Hyst_{dynamic}$, and $TTT_{dynamic}$ are analyzed using numerical simulation. Then, the performance of the proposed self-optimizing HCPs is analyzed and compared with the existing HCPs optimization methods. All

methods and parameters are implemented using MATLAB® R2021b with the assistance of Communications Toolbox, Antenna Toolbox, and 5G Toolbox. For handover performance analysis, Event A2 and Event A3 are used. Event A2 represents the *serving cell-based HCP optimization* and absolute handover measurement strategy; and Event A3 represents the *target cell-based HCP optimization* and relative handover measurement strategy.

A. SIMULATION SETUP AND PARAMETER

The proposed self-optimizing HCPs are tested in a 5G environment for FR1 (Sub-6 5G frequency band). We assume a single tier 5G network consisting of small (micro) cells with a cell radius of 200 m. The small cells have an omnidirectional antenna operating at 3.5 GHz (n78 5G band). The small cells are deployed on an area of size of 0.6 km × 0.6 km with significant coverage overlapping between adjacent cells to ensure the MS can discover multiple small cells while camped on a serving cell. Fig. 6 depicts the deployment scenario, and Table 3 shows the system and environmental parameter settings. The starting point of MS route/trajectory and MS location in the network follows a random distribution.

A directional mobility model is used which is common in vehicular speed scenarios. A mobile system (MS) will traverse the trajectory from beginning to end (source/destination) with various speeds up to 120 km/h. Simulation is repeated for $\mathcal{K}$ number of trajectories; each randomly generated with a random MS starting point. The environmental and system parameters used are summarized in Table 2 [10], [16], [33].

B. HANDOVER KEY PERFORMANCE INDICATORS (KPI)

To evaluate the performance of the proposed method, four standard performance metrics, namely Handover Rate (HOR), Ping-Pong Handover Rate (PPHR), Handover Failure Rate (HFR) and Mean Throughput ($\mathcal{T}$) are measured, as here defined.

1) HANDOVER RATE (HOR)

The *HOR* describes the frequency at which handover occurs. It is given by the ratio of number of handovers and running time per user. The higher HOR decreases system performance. The HOR is given by (24).

$$\text{HOR} = \frac{\sum_{k=1}^{\mathcal{K}} N_k^{\text{HO}}}{\sum_{k=1}^{\mathcal{K}} T_k} \tag{24}$$

where N_k^{HO} and T_k are number of handovers and user running time on route k.

2) PING-PONG HANDOVER RATE (PPHR)

The PPHR describes the frequency at which ping-pong handover occurs. Ping-pong handover refers to a phenomenon when the MS handovers back and forth between a serving and target cell pair several times before it settles the attachment to the target cell. The ping-pong effect is common at the overlapping area of the cell pair due to high signal fluctuation and a *too-early* handover decision is being made. The higher PPHR may result in poor user experience. The PPHR is given by the ratio of number of handover ping-pong and running time per user as shown in (25).

$$\text{PPHR} = \frac{\sum_{k=1}^{\mathcal{K}} N_k^{\text{PP}}}{\sum_{k=1}^{\mathcal{K}} T_k} \tag{25}$$

where N_k^{PP} is number of ping-pong handovers on route k.

3) HANDOVER FAILURE RATE (HFR)

The HFR describes the frequency at which handover failure occurs. Handover failures refer to a phenomenon when the MS initiates the handover but fails to complete the handover process. Typically, this might happen when (a) MS experiences poor coverage and triggers a handover procedure to a target cell then subsequently moves to a better coverage or target before the previous handover procedure is completed. For example, Event A1 can be used to cancel the ongoing handover. (b) MS exists serving cell before the handover is completed due to the handover decision being made either *too-late*, or to the *wrong-cell*. This is a common problem in small cells, especially for MS moving at high speed. The higher HFR is more severe to system performance. The HFR is given by the ratio of number of handover failures and running time per user as shown in (26).

$$\text{HFR} = \frac{\sum_{k=1}^{\mathcal{K}} N_k^{\text{HF}}}{\sum_{k=1}^{\mathcal{K}} T_k} \tag{26}$$

where N_k^{HF} is number of handover failures on route k.

4) AVERAGE THROUGHPUT

Throughput refers to the amount of data that can be transferred per unit time, measured in Mbps. The higher value indicates higher system performance. The 5G NR throughput can be estimated theoretically using 3GPP formula (27) [34].

$$\mathcal{T} = 10^{-6} * \sum_{j=1}^{J} \left(\mathcal{L}_m \mathcal{M}_Q \beta \left(\frac{\mathcal{R}}{1024}\right) \left(\frac{\mathcal{N}_{\text{PRB}}^{\mu} * 12}{t_s^{\mu}}\right) (1 - \mathcal{Q}) \right) \tag{27}$$

where J is the number of aggregated Component Carriers (CCs), $\mathcal{L}_m$ is number of MIMO layers, $\mathcal{M}_Q$ is Modulation order, $\mathcal{R}$ is Code rate, β is Scaling factor given as 1, 0.8, 0.75, or 0.4 depending on CCs (it is 1 for 1 CC), $\mathcal{N}_{\text{PRB}}^{\mu}$ is number of Physical Resource Blocks per given numerology μ, t_s^{μ} is symbol duration in a subframe for numerology μ given by $t_s^{\mu} = 1/(2^{\mu} * \text{symbols per slot})$ milliseconds, and $\mathcal{Q}$ is Overhead from control channels estimated at 0.14 for downlink (DL) and 0.08 for uplink (UL) for FR1 [34].

We used n78 5G band in numerology 1 ($\mu = 1$) with normal cyclic prefix, without carrier aggregation. The modulation order $\mathcal{M}_Q$ and code rate $\mathcal{R}$ are obtained using SINR. The SINR is used to compute spectral efficiency which is

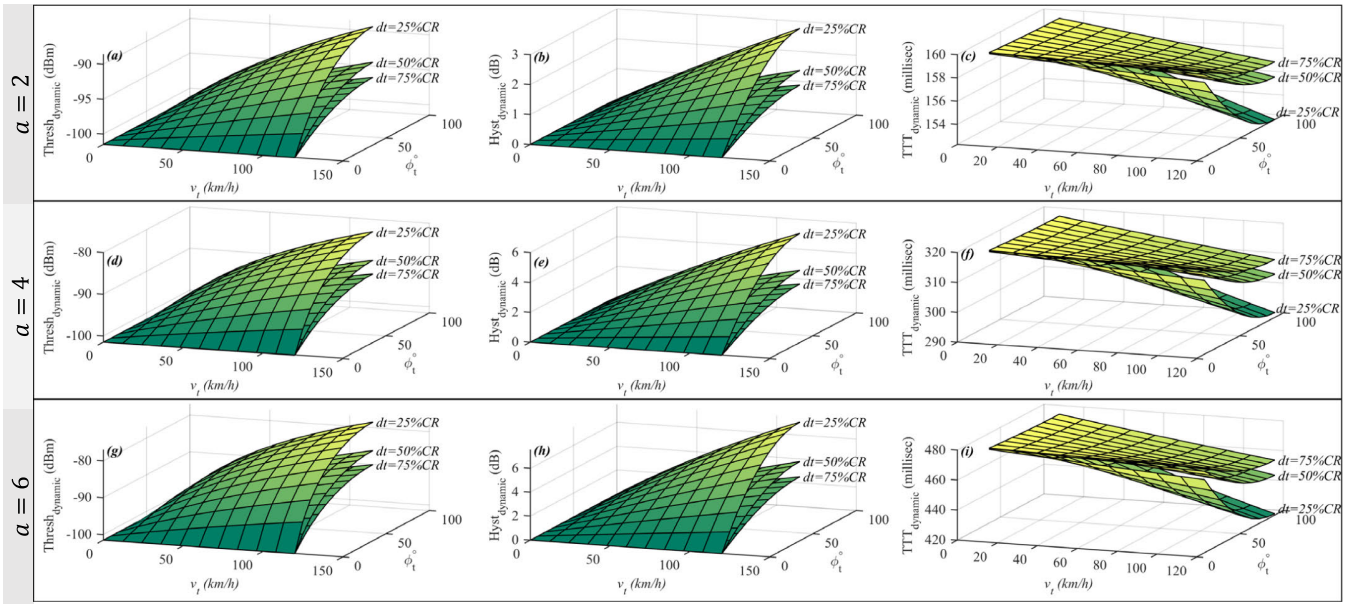

FIGURE 7. Serving cell-based ($\epsilon = 1$) self-optimizing Handover Control Parameters (HCPs) with respect to the MS moving speed and the MS angle of direction, at the MS to BS separation distance 25%, 50%, and 75% of cell radius (CR), for the handover window time coefficient a of 2, 4 and 6.

given by ln(1 + SINR) in nats/s/Hz where 1 nat = 1/ln(2) = 1.4427 bits) [35], [36]. The spectral efficiency is then used to determine Modulation and Coding Scheme (MCS), $\mathcal{M}_Q$ and $\mathcal{R}$ using 3GPP lookup table [37].

In Section VI-C, we analyze the proposed $Thresh_{dynamic}$, $Hyst_{dynamic}$, and $TTT_{dynamic}$ using numerical simulations; whereas the performance of the proposed $Thresh_{dynamic}$, $Hyst_{dynamic}$, and $TTT_{dynamic}$ in terms of handover is presented in Section VI-D using the 4 KPIs discussed in this section.

C. SELF-OPTIMIZING HCPs NUMERICAL ANALYSIS

Based on the proposed self-optimizing HCPs in Section V, the effect of various parameters on the $Thresh_{dynamic}$, $Hyst_{dynamic}$, and $TTT_{dynamic}$ as presented in (17), (19), and (23), respectively, have been analyzed and compared by numerical simulation for *serving cell-based HCP optimization* ($\epsilon = 1$) and for *target cell-based HCP optimization* ($\epsilon = -1$). In what follows, some parameters are configured as: the system and environmental parameters, namely the minimum reference received power $Q_{rxlevmin}$ is −101.5 dBm, the handover RRC signalling delay (handover latency) τ is 1 s, the MS measurement periodicity ψ is 160 ms and the propagation path loss factor n is 3.5 (for urban environment); the handover window time coefficients a is 2, 4 and 6; the MS moving speed v is ranging from 0 to 120 km/h with an increment of 10 km/h; the MS direction angle ϕ is ranging from 0° to 90°; the MS to BS separation distance d is 50 m, 100 m and 150 m which are 25%, 50% and 75% of cell radius.

Fig. 7 shows the *serving cell-based HCP optimization* ($\epsilon = 1$) for different values of handover window coefficient a. Fig. 7(a)-(c) for $a = 2$; Fig. 7(d)-(f) for $a = 4$; and Fig. 7(g)-(i) for $a = 6$. Larger values of a means a wider handover window with higher dynamic range and higher peak values for $Thresh_{dynamic}$, $Hyst_{dynamic}$, and $TTT_{dynamic}$ compared to smaller values of a. The $a = 2$ is a baseline value as established in Section V-A. It gives a narrow handover window that accommodates *inbound* and *outbound* handover. The $a = 2$ will be used for handover simulation. The advantage of a narrow handover window in *serving cell-based* handover measurements is that a lesser chance of unnecessary handover and ping pong handover exist with narrow handover than with a wider window. For example, if we recall the timing analysis in Section V-C as illustrated in Fig. 5., Hysteresis margin and Time-To-Trigger at maximum occupy 24% of the maximum time window $a\tau$ (when $x = 0.5$) while reserving 76% for handover procedures. With a narrow handover window such as $a = 2$, 76% of $a\tau$ will mean 1.52 s is reserved for handover, which is higher than handover latency τ of 1 s and time remainder of 520ms before MS exits cell $Q_{rxlevmin}$ exposing MS to less unnecessary handover and ping pong handover. With a wider handover window such as $a = 4$, the $a = 2a = 4a = 6$ 76% of $a\tau$ will mean 3.04 s is reserved for handover (much higher than handover latency τ of 1 s) with time remainder of 2.04 s before MS exits cell $Q_{rxlevmin}$, exposing MS to more unnecessary handover and ping pong handover. This explains why the industrial practice of vendor-predefined fixed HCPs underperforms. When small values of Thresholds and Hysteresis (narrow window) are used, the user moving at a fast speed is anticipated to exit the cell sooner and, therefore, exposed to a higher probability of handover failure and vice versa.

The proposed dynamic self-optimizing HCPs for *serving cell-based HCP optimization* ($\epsilon = 1$) presented in Fig. 7, shows the trends for $Thresh_{dynamic}$, $Hyst_{dynamic}$ and

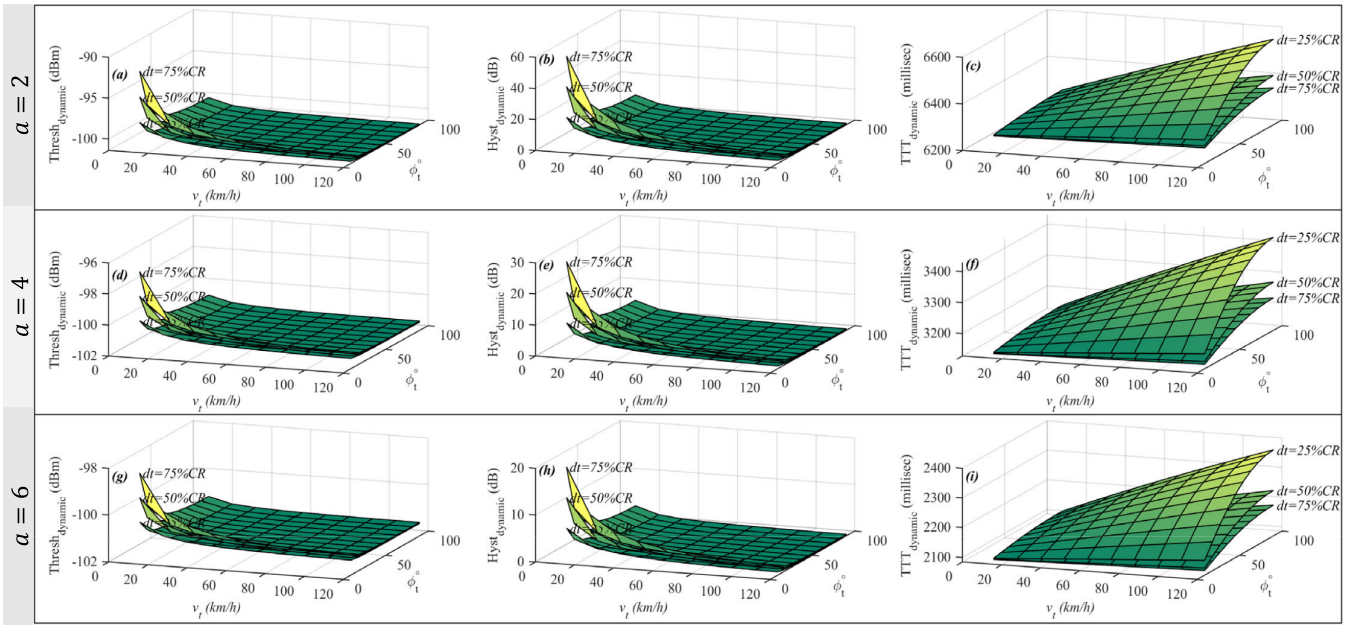

FIGURE 8. Target cell-based ($\epsilon = -1$) self-optimizing Handover Control Parameters (HCPs) with respect to the MS moving speed and the MS angle of direction, at the MS to BS separation distance 25%, 50%, and 75% of cell radius (CR), for the handover window time coefficient a of 2, 4, and 6.

$TTT_{dynamic}$, which are similar from narrow window ($a = 2$) to wider window ($a = 6$). The trend indicates that at higher MS speed, larger region and smaller trigger time are reserved for handover to be performed successfully, while at lower MS speed, smaller region and longer trigger time are reserved for handovers as slow-moving user will take relatively longer time to cross a small region than a fast-moving user.

Additionally, it is observed in Fig. 7 that $Thresh_{dynamic}$ and $Hyst_{dynamic}$ increase while the $TTT_{dynamic}$ decreases as: MS speed increases, MS direction angle increases, and MS-BS separation distance decreases. This means near the BS (e.g., at 25% cell radius or less) higher $Thresh_{dynamic}$ and $Hyst_{dynamic}$; and lower $TTT_{dynamic}$ are yielded, while at the cell edge (e.g., at 75% cell radius or higher) lower $Thresh_{dynamic}$ and $Hyst_{dynamic}$; and higher $TTT_{dynamic}$ are produced. The $Thresh_{dynamic}$, $Hyst_{dynamic}$ and $TTT_{dynamic}$ are complementary.

Regarding the MS angle of direction, 0° means the MS is moving around the serving BS, neither towards the serving BS nor away, hence the HCPs $\{Thresh_{dynamic}, Hyst_{dynamic}, TTT_{dynamic}\}$ are at {minimum, minimum, maximum} i.e., $\{Q_{rxlevmin}, 0, xa\psi\}$. As observed in Fig. 7, similar HCPs values are achieved when MS is stationary. These can be regarded as baseline HCP values for any handover window time coefficients a. As the MS angle of direction increases from 0° to maximum, it means that the MS is moving towards the serving BS where signal strength increases substantially, reaching a maximum increase at the perpendicular direction (90°). These substantial increase in the MS angle of direction for a given nonzero MS speed yields a substantial increase of $Thresh_{dynamic}$ and $Hyst_{dynamic}$; and decrease of $TTT_{dynamic}$.

Generally, the $Thresh_{dynamic}$, $Hyst_{dynamic}$ and $TTT_{dynamic}$ complements each other when $Thresh_{dynamic}$, and $Hyst_{dynamic}$ increase, $TTT_{dynamic}$ decrease. To further understand the inverted nature of $TTT_{dynamic}$ as shown in say Fig. 7(c); given MS measurement periodicity $\psi = 160$ ms and handover latency $\tau = 1$ s; the handover window time coefficient $a = 2$ yields a maximum limit handover window $a\tau$ of 2 s and a maximum limit of Time-To-Trigger $xa\psi$ of 160 ms for any MS speed (refer to Fig. 5 where x is 50 percentile), which is the highest bound of $TTT_{dynamic}$ for all variations of parameters within the given range for $a = 2$. It can be noted that, with $a = 2$, the maximum limit of Time-To-Trigger becomes equal to MS measurement periodicity ψ. Since MS measurement periodicity is higher than the SSB burst periodicity, then MS will be capable of monitoring a certain number of measurements before Time-To-Trigger expires. This result provides a basic guideline to evaluate the Time-To-Trigger for any choice of the handover window time coefficient a.

Lastly Fig. 7 illustrates the dynamic self-optimized HCPs reaching their peak values at maximum MS speed (120 km/h) for $Thresh_{dynamic}$ and $Hyst_{dynamic}$, and at minimum MS speed (0 km/h) for $TTT_{dynamic}$. The trend presented in Fig. 7 applies only in *serving cell-based HCP optimization* which includes events A1 and A2; and event A5 and B2 as shown in Table 2.

Fig. 8 shows the *target cell-based HCP optimization* ($\epsilon = -1$) for different values of a where Fig. 8(a)-(c) are obtained when $a = 2$; Fig. 8(d)-(f) when $a = 4$; and Fig. 8(g)-(i) when $a = 6$. The trends are opposite to the *serving cell-based HCP optimization* ($\epsilon = 1$) presented in Fig. 7, and they apply only in handover measurement strategy based on events A3, A4, B1, and A6; and events A5 and B2 as shown in Table 2.

In *target cell-based HCP optimization,* the HCPs are obtained based on the system parameters of target cells, and they are applied to signal measurements from target cells using the handover event of choice. It can be observed in Fig. 8 that $Thresh_{dynamic}$ and $Hyst_{dynamic}$ decrease while the $TTT_{dynamic}$ increase when: MS speed increases, MS direction angle increases, and MS-BS separation distance decreases. This means near target cell BS (e.g., at 25% cell radius), lower values of $Thresh_{dynamic}$ and $Hyst_{dynamic}$ and higher values $TTT_{dynamic}$ are produced. Considering two overlapping cells, the 'near target cell BS' situation is mostly encountered at the edge of the serving cell. By lowering the target cell's Threshold and Hysteresis increases the chance of successful handovers. In the contrary, near the edge of target cell (e.g., 75% cell radius), higher values of $Thresh_{dynamic}$ and $Hyst_{dynamic}$ and lower values of $TTT_{dynamic}$ are produced. For overlapping cells, the 'near edge of target cell' situation is encountered at region near the serving BS than cell edge. Therefore, increasing the target cell Threshold and Hysteresis reduces the chance of unnecessary handovers and ping-pong handovers. Similar to Fig. 7, the self-optimizing $Thresh_{dynamic}$, $Hyst_{dynamic}$ and $TTT_{dynamic}$ in *target cell-based HCP optimization* are also complementary as shown in Fig. 8. It is also important to note that the *target cell-based HCP optimization* in Fig. 8 shows higher peak values for $a = 2$ and the peak values reduce as a increases to $a = 6$. This is due to the multiplicative inverse. Therefore, the narrow handover window for the *target cell-based HCP optimization* will be $a \gg 2$. With $a = 6$ as shown in Fig. 8(g)-(i), the $Thresh_{dynamic}$, $Hyst_{dynamic}$ and $TTT_{dynamic}$ ranges are $[Q_{rxlevmin}, -98]$ dBm, [0, 20] dB, and [2.1, 2.4] s respectively, while for larger $a = 8$ showed $[Q_{rxlevmin}, -99]$ dBm, [0, 15] dB, and [1.5, 1.8] s. Therefore, the choice to which value of handover window coefficient to use for target cell-based measurement events such as A3, A4, B1 and A6; and event A5 and B2, as shown in Table 2 is left to the network operator. This is because the *target cell-based HCP optimization* is not bound to a serving cell. However, the type of cell deployment can give insight into how to select the handover window coefficient for the case. For example, in an ultra-dense network (UDN) where multiple cells are available even very close to serving cell BS, stringent HCP policy such as in Fig. 8(a)-(c) where $a = 2$ can be applied, while in much less dense deployment a much less stringent HCP policy such as in Fig. 8(g)-(i) where $a = 6$ or higher can be applied.

Fig. 8 also illustrates the dynamic self-optimized HCPs reaching their peak values with respect to MS speed and MS angle of direction at ∼0 km/h and ∼0° for $Thresh_{dynamic}$ and $Hyst_{dynamic}$; and at 120 km/h and 90° for $TTT_{dynamic}$. stricter HCP policy is obtained for slow-moving users, that is, {maximum, maximum, minimum} for $\{Thresh_{dynamic}, Hyst_{dynamic}, TTT_{dynamic}\}$ is obtained for application to target-based handover measurements. This implies that maximizing the target Threshold and Hysteresis margin for a slow-moving user will minimize *too-early* handovers and hence unnecessary handovers and ping pong effect. Meanwhile, for fast-moving users, the {minimum, minimum, maximum} HCP policy for $\{Thresh_{dynamic}, Hyst_{dynamic}, TTT_{dynamic}\}$ is obtained, which implies that minimizing the target Threshold and Hysteresis margin for a fast-moving user will minimize *too-late* handovers and handover failures.

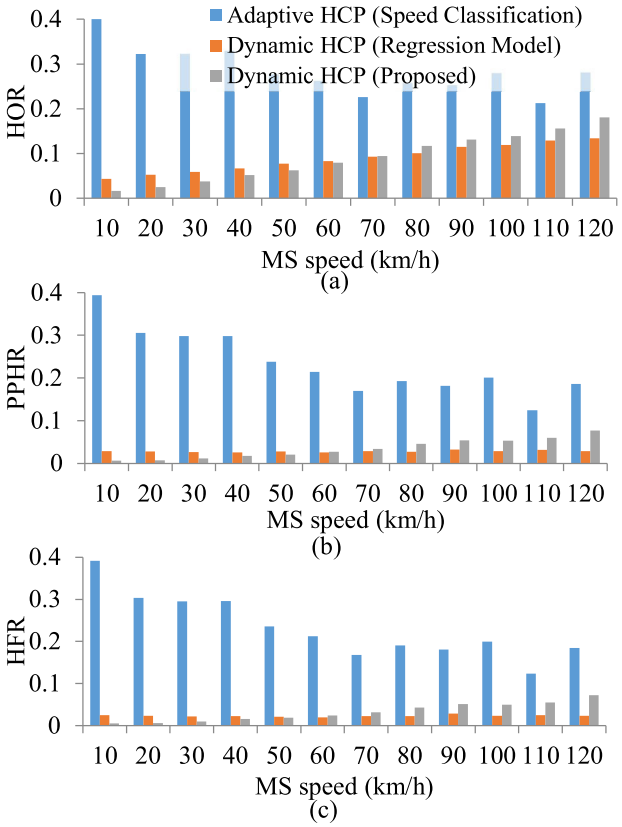

FIGURE 9. Handover performance of self-optimizing HCPs based on *serving cell-based HCP optimization* using Event A2, in comparison with adaptive HCP method using speed classification and dynamic HCP method using regression model. (a) Handover Rate (*HOR*), (b) Ping-pong Handover Rate (*PPHR*), and (c) Handover Failure Rate (*HFR*).

D. HANDOVER PERFORMANCE ANALYSIS

We analyzed the performance of self-optimizing HCPs by implementing it in MATLAB® R2021b. The network layout is in a 0.6 km × 0.6 km size as shown in Fig. 6. The 5G urban micro-cell test environment was constructed using Antenna Toolbox functions such as RF transmitter site *txsite*; RF receiver site *rxsite*; received signal strength sigstrength; propagation model propagationModel; path loss of radio wave propagation pathloss and signal-to-interference-plus-noise ratio (SINR) sinr. The antenna is modelled using Phased Array System Toolbox with isotropic antenna element *phased.IsotropicAntennaElement*. The close-in propagation model [30] is used. The transmitter site (BS) and receiver site (MS) locations are defined using a cartesian coordinate system. The number of BS is 4, and thus 4 cells are formed in the network with substantial overlapped coverage, as shown

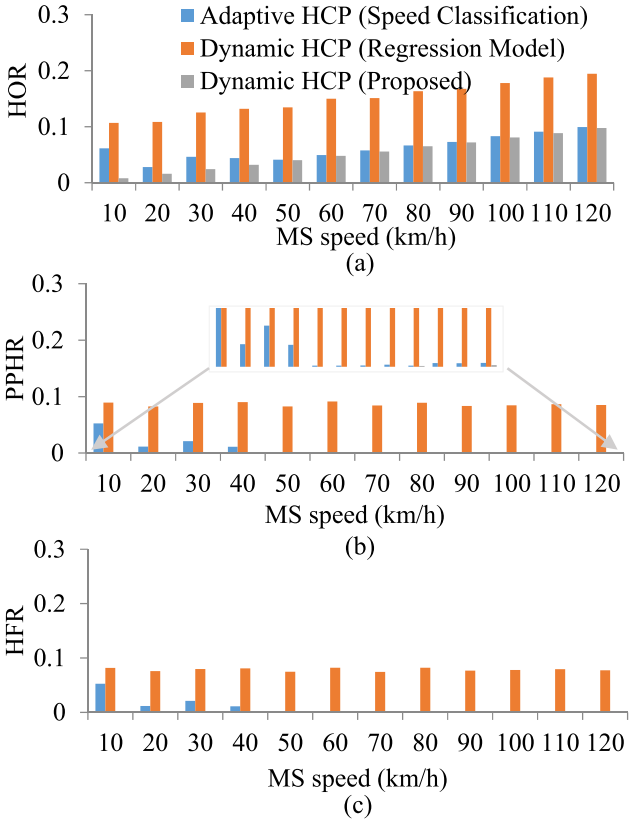

FIGURE 10. Handover performance of self-optimizing HCPs based on *target cell-based HCP optimization* using Event A3, in comparison with adaptive HCP method using speed classification and dynamic HCP method using regression model. (a) Handover Rate (*HOR*), (b) Ping-pong Handover Rate (*PPHR*), and (c) Handover Failure Rate (*HFR*).

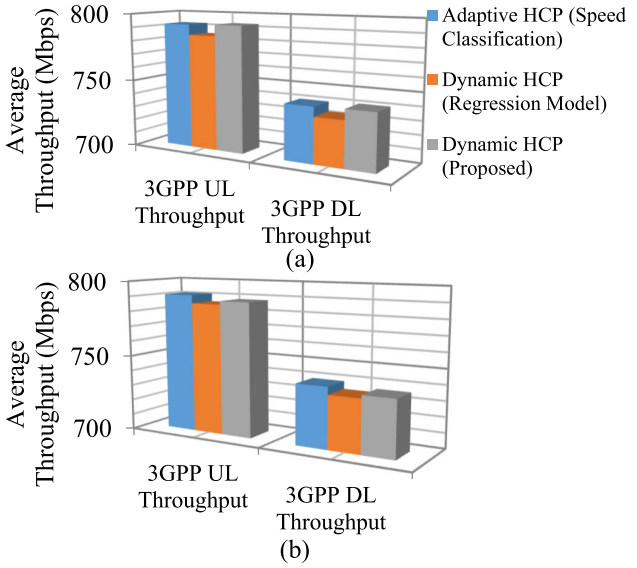

FIGURE 11. Average 3GPP uplink (UP) and downlink (DL) throughput of proposed self-optimizing HCPs based on (a) *serving cell-based HCP optimization* using Event A2, and (b) *target cell-based HCP optimization* using Event A3, in comparison with adaptive HCP method using speed classification and dynamic HCP method using regression model.

in Fig. 6. The number of MS is 1, which is placed randomly along the y-coordinate axis of the network layout. The MS traverses the network with different speeds ranging from 0 to 120 km/h using directional mobility. The MS acquires RSSI and SINR at its current location for all available BS whereby RSRP and RSRQ are estimated using a number of physical resource block (PRB) [38]. The SINR is used to estimate average throughput as (27) using properties of RF transmitter, RF receiver, and antenna elements defined in the test environment. Other systems and environmental parameters used are defined in Table 3.

At the beginning of the simulation, 200 MS trajectories' starting points are generated by using a homogeneous Poisson point process on a 0.03 km $\times$ 0.6 km of the network layout. The MS is placed at the starting point of each trajectory and traverses the network to the end of the network layout for all 200 trajectories with MS speed ranging 0 – 120 km/h. Handover is evaluated by applying self-optimizing HCPs accordingly, as shown in Fig. 2 for both *serving cell-based HCP optimization*($\epsilon = 1$) and *target cell-based HCP optimization*($\epsilon = -1$) using Event A2 and Event A3 respectively.

A handover is counted when the handover event is qualified and the corresponding $TTT_{dynamic}$ is expired. The handover procedure consumes time equivalent to RRC signaling delays from *Step 2* to *Step 8* shown in Fig. 1. This is referred as handover latency τ, $\tau = 1$s is used for simulation. Handover failure is counted when: A handover request to a new target is sent, and ongoing handover is cancelled; or when serving cell's radio link quality falls below the minimum (out of reach) before a handover is completed; when each occur before timer τ of an ongoing handover expires. Meanwhile, ping-pong handover is counted when back-and-forth handover between two cells occurs within a certain time, a time threshold of 1 s is used [22].

The handover performance of the proposed self-optimizing HCPs is evaluated in terms of four KPIs, namely Handover Rate (*HOR*), Ping-pong Handover Rate (*PPHR*), Handover Failure Rate (*HFR*), and Average Throughput ($\mathcal{T}$) defined in Section VI-B. Results are compared with adaptive HCP using speed classification [15] and dynamic HCP using a regression model [26].

Fig. 9 shows the handover performance result of the proposed self-optimizing HCPs method based on *serving cell-based HCP optimization* using Event A2, in comparison with the adaptive HCP method using speed classification and dynamic HCP method using regression model.

As shown in Fig. 9, the proposed method outperforms both the dynamic HCP (regression model) and the adaptive HCP (speed classification) approaches in terms of HOR, PPHR, and HFR for MS speed of approximately 70 km/h and lower. At this MS speed range, the average HOR of 0.3200, 0.0637 and 0.0455; PPHR of 0.2913, 0.0268 and 0.0150; and HFR of 0.2890, 0.0225 and 0.0130 were achieved for the adaptive HCP (speed classification), the dynamic HCP (regression model) and the proposed self-optimizing

HCP methods, respectively. This indicates that the proposed method has improved handover performance by 85.75%, 94.85% and 95.50% for HOR, PPHR and HFR, respectively, in comparison with the adaptive HCP (speed classification) approach; and by 28.57%, 44.03% and 42.22% for HOR, PPHR and HFR, respectively, in comparison with the dynamic HCP (regression model) approach for MS speed of 70 km/h and lower.

Overall performance indicates the average HOR of 0.2861, 0.0894 and 0.0909; PPHR of 0.2337, 0.0282 and 0.0345; and HFR of 0.2317, 0.0234 and 0.0317 were achieved for the adaptive HCP (speed classification), the dynamic HCP (regression model) and the proposed self-optimizing HCP methods, respectively. This indicates that the proposed method has improved overall performance by 68.23%, 85.24% and 86.32% for HOR, PPHR and HFR, respectively, in comparison with the adaptive HCP (speed classification) approach. Meanwhile, it shows reduced overall performance by 1.68%, 22.34% and 35.47% for HOR, PPHR and HFR, respectively, in comparison with the dynamic HCP (regression model) approach. This is due to the increase of HOR, PPHR, and HFR for MS speeds above 70 km/h. In theory, similar performance is anticipated for other *serving cell-based HCP optimization* related events such as A1 and part of A5 and B2.

The decrease in handover performance of proposed method for *serving cell-based HCP optimization* for MS speed above 70 km/h could be caused by the assumption of $x = 0.5$ in (23) which is discussed in Section V-C. As illustrated in Fig. 5, $x = 0.5$ will bound $TTT_{dynamic}$ at $xa\psi/2$, which will be slightly reduced at higher MS speed, as shown in Fig. 7(c). The smaller upper bound of $TTT_{dynamic}$ will result in high PPHR and HFR at the overlapping region of serving and target cells. To mitigate this, further improvement can be made for the *serving cell-based HCP optimization* case such as making x dynamic so that to scale the upper bound of $TTT_{dynamic}$ with say MS speed.

In Fig. 10, we provide the handover performance for *target cell-based HCP optimization* using Event A3, the proposed self-optimizing HCP approach has outperformed both the adaptive HCP method using speed classification and the dynamic HCP method using regression model methods for all MS speed tested.

Overall performance indicates that the average HOR of 0.0617, 0.1500 and 0.0524; PPHR of 0.0088, 0.0866 and 0.0001; and HFR of 0.0086, 0.0784 and 0.0001 were achieved for the adaptive HCP (speed classification), the dynamic HCP (regression model), and the proposed self-optimizing HCP methods, respectively.

This indicates an overall performance gain of the proposed method by 15.07%, 98.86% and 98.84% for HOR, PPHR and HFR, respectively, in comparison with the adaptive HCP (speed classification) approach; and a performance gain by 66.92%, 99.89% and 99.87% for HOR, PPHR and HFR, respectively, in comparison with the dynamic HCP (regression model) approach. The higher gain in PPHR and HFR indicates the proposed method can highly minimize unnecessary handovers and failures. Worst performances are shown by the dynamic HCP method using a regression model, this could be due to the fact that the regression model did not take into account sufficient parameters to cope with system dynamic, only inter-site distance and angle of MS movements were used. This risk worsens handover performance, especially in target cell-based events such as A3, where serving cell condition doesn't control the handover necessity estimation. Therefore, risking MS leaving serving cell before handover is completed.

In Fig. 11 we provide overall average throughput (uplink (UP) and downlink (DL)) based on 3GPP throughput estimation formular in (27), for the proposed self-optimizing HCPs based on *serving cell-based HCP optimization* using Event A2, and *target cell-based HCP optimization* using Event A3. The results are compared with the adaptive HCP method using speed classification and the dynamic HCP method using regression model.

In terms of average achievable throughput based on *serving cell-based HCP optimization* using Event A2, as shown in Fig. 11 (a), the proposed method achieved approximately 793 Mbps uplink throughput, while the adaptive HCP method using speed classification achieved 792 Mbps and the dynamic HCP method using regression model achieved 785 Mbps, respectively. In terms of the downlink throughput, 741 Mbps is achieved by the proposed method, while the adaptive HCP method using speed classification achieved 740 Mbps and the dynamic HCP method using regression model achieved 734 Mbps respectively. For the case of *target cell-based HCP optimization* using Event A3, the proposed method achieved approximately 788 Mbps uplink and 735 Mbps downlink, respectively, with marginal performance differences in comparison to other methods, as shown in Fig. 11 (b).

Although the throughput improvement is marginal, this is an important result, since it indicates that the proposed method can provide higher data rates for both *serving cell-based HCP optimization* and *target cell-based HCP optimization* related events without the need for network operators to perform manual tuning.

VII. CONCLUSION AND FUTURE WORK

In this paper, we proposed a self-optimization method for three main handover control parameters (HCPs), namely Threshold, Hysteresis, and Time-To-Trigger that considers the channel conditions, user mobility, and system parameters to determine the optimal values of HCPs to improve handover performance in 5G wireless networks. We proposed closed-form analytical expressions which provide relationship between user mobility, channel conditions, and system parameters to each of the three HCP. This allowed the proposed method to be cell-specific, where the HCPs can be self-optimized based on the type of cell and its associated

radio link and system configuration. To this end, we classified 3GPP handover measurement events as either serving cell-based (event A1, A2), target cell-based (A3, A4, B1 and A6), or both (A5 and B2) based on a cell's measurements to be used to acquire self-optimized HCPs. All input parameters to the proposed method are taken from current measurements performed by the MS, and manual tuning is not required which is a popular technique in the literature. For evaluation purposes, we selected events A2 and A3 to represent serving cell-based and target cell-based, respectively.

The results show significant improvements in handover performance in terms of Handover Rate (HOR), Ping-Pong Handover Rate (PPHR), and Handover Failure Rate (HFR) compared to existing HCP optimization approaches based on speed classification and regression model. In serving cell-based events (A2), the method demonstrates enhanced handover efficiency at speeds below 70 km/h, making it well-suited for low-mobility scenarios and urban vehicular mobility. Similarly, in target cell-based events (A3), the proposed approach exhibits improved handover performance across a wide range of MS speeds, up to 120 km/h. This suggests its adaptability and effectiveness in diverse scenarios. Notably, the proposed self-optimizing HCP approach maintains a stable throughput performance for both serving and target cell-based events, reinforcing its viability as an automatic optimization solution for fifth-generation wireless communication.

From the analysis, future work of the proposed method will be to improve performance for the *serving cell-based HCP optimization* case, which has shown a decline for the MS speed of above 70 km/h. In general, handover parameter automatic self-optimization is significant for Load Balancing Optimization (LBO) and Mobility Robustness Optimization (MRO), which are functions designed for automatic configuration and update of HCPs to improve the handover performance in 5G networks and beyond 5G. There are several further research directions that can be taken such as the implementation of automatic self-optimization of HCPs in millimeter wave, massive MIMO, dual connectivity, ultra-densification and moving networks.

APPENDIX A
LIST OF ABBREVIATIONS

Abbreviation	Full Form
3GPP	3rd Generation Partnership Project
4G	Fourth Generation Cellular Networks
5G	Fifth Generation Cellular Networks
AMF	Access and Mobility Management Function
BS	Base Stations
CC	Component Carrier
C-RNTI	Cell Radio Network Temporary Identifier
DAPS	Dual Active Protocol Stack
DL	Downlink
DRB	Data Radio Bearer
HCP	Handover Control Parameters
HFR	Handover Failure Rate
HOR	Handover Rate
KPI	Key Performance Indicators
LBO	Load Balancing Optimization
LOS	Line-of-Sight
LTE-A	Long-Term Evolution-Advanced
MCS	Modulation and Coding Scheme
MR	Measurement Report
MRO	Mobility Robustness Optimization
MS	Mobile Station
MIMO	Multiple-Input Multiple-Output
NLOS	Non-Line-of-Sight
NR	New Radio
PPHR	Ping-Pong Handover Rate
PRB	Physical Resource Block
QoS	Quality of Service
RACH	Random Access Channel
RF	Radio Frequency
RRC	Radio Resource Control
RRM	Radio Resource Management
RSRP	Reference Signal Received Power
RSRQ	Reference Signal Received Quality
RSSI	Received Signal Strength Indicator
SIB	System Information Block
SMTC	Synchronization Signal Block (SSB) based Measurement Timing Configuration
SON	Self-Organizing Network
SSB	Synchronization Signal Block
SINR	Signal-to-Interference-plus-Noise Ratio
UDN	Ultra-Dense Network
UL	Uplink
UPF	User Plane Function

REFERENCES

[1] X. Ge, J. Ye, Y. Yang, and Q. Li, "User mobility evaluation for 5G small cell networks based on individual mobility model," *IEEE J. Sel. Areas Commun.*, vol. 34, no. 3, pp. 528–541, Mar. 2016, doi: 10.1109/JSAC.2016.2525439.

[2] *5G; NR; Radio Resource Control (RRC); Protocol Specification*, 3GPP Standard TS 38.331, Version 16.1.0, Release 16, 2020.

[3] K. Sun, J. Yu, W. Huang, H. Zhang, and V. C. M. Leung, "A multi-attribute handover algorithm for QoS enhancement in ultra dense network," *IEEE Trans. Veh. Technol.*, vol. 70, no. 5, pp. 4557–4568, May 2021, doi: 10.1109/TVT.2021.3070337.

[4] M. I. Goh, A. I. Mbulwa, H. T. Yew, A. Kiring, S. K. Chung, A. Farzamnia, A. Chekima, and M. K. Haldar, "Handover decision-making algorithm for 5G heterogeneous networks," *Electronics*, vol. 12, no. 11, p. 2384, May 2023, doi: 10.3390/ELECTRONICS12112384.

[5] S. K. Chung, M. I. Goh, H. T. Yew, B. L. Chua, S. S. Husain, and A. I. Mbulwa, "Enhanced bandwidth based handover decision making algorithm for small cell wireless networks," in *Proc. IEEE 2nd Int. Conf. Artif. Intell. Eng. Technol. (IICAIET)*, Sep. 2020, pp. 1–6, doi: 10.1109/IICAIET49801.2020.9257853.

[6] Y. Zhang and B.-H. Soong, "Handoff dwell time distribution effect on mobile network performance," *IEEE Trans. Veh. Technol.*, vol. 54, no. 4, pp. 1500–1508, Jul. 2005, doi: 10.1109/TVT.2005.851374.

[7] H. T. Yew, A. Chekima, A. Kiring, A. I. Mbulwa, J. A. Dargham, and S. K. Chung, "RSS based vertical handover schemes in heterogeneous wireless networks: Past, present & future," in *Proc. IEEE 2nd Int. Conf. Artif. Intell. Eng. Technol. (IICAIET)*, Sep. 2020, pp. 1–5, doi: 10.1109/IICAIET49801.2020.9257844.

[8] M. Manalastas, M. U. B. Farooq, S. M. A. Zaidi, A. Abu-Dayya, and A. Imran, "A data-driven framework for inter-frequency handover failure prediction and mitigation," *IEEE Trans. Veh. Technol.*, vol. 71, no. 6, pp. 6158–6172, Jun. 2022, doi: 10.1109/TVT.2022.3157802.

[9] F. Guidolin, I. Pappalardo, A. Zanella, and M. Zorzi, "Context-aware handover policies in HetNets," *IEEE Trans. Wireless Commun.*, vol. 15, no. 3, pp. 1895–1906, Mar. 2016, doi: 10.1109/TWC.2015.2496958.

[10] W. Huang, M. Wu, Z. Yang, K. Sun, H. Zhang, and A. Nallanathan, "Self-adapting handover parameters optimization for SDN-enabled UDN," *IEEE Trans. Wireless Commun.*, vol. 21, no. 8, pp. 6434–6447, Aug. 2022, doi: 10.1109/TWC.2022.3149415.

[11] Y. Sun, W. Jiang, G. Feng, P. V. Klaine, L. Zhang, M. A. Imran, and Y.-C. Liang, "Efficient handover mechanism for radio access network slicing by exploiting distributed learning," *IEEE Trans. Netw. Service Manage.*, vol. 17, no. 4, pp. 2620–2633, Dec. 2020, doi: 10.1109/TNSM.2020.3031079.

[12] *5G; Management and Orchestration; Self-Organizing Networks (SON) for 5G Networks*, 3GPP Standard TS 28.313, Version 17.4.0, Release 17, 2022.

[13] W. Tashan, I. Shayea, S. Aldirmaz-Colak, M. Ergen, M. H. Azmi, and A. Alhammadi, "Mobility robustness optimization in future mobile heterogeneous networks: A survey," *IEEE Access*, vol. 10, pp. 45522–45541, 2022, doi: 10.1109/ACCESS.2022.3168717.

[14] A. Alhammadi, M. Roslee, M. Y. Alias, I. Shayea, S. Alriah, and A. B. Abas, "Advanced handover self-optimization approach for 4G/5G HetNets using weighted fuzzy logic control," in *Proc. 15th Int. Conf. Telecommun. (ConTEL)*, Jul. 2019, pp. 1–6, doi: 10.1109/CONTEL.2019.8848507.

[15] A. Alhammadi, M. Roslee, M. Y. Alias, I. Shayea, S. Alraih, and K. S. Mohamed, "Auto tuning self-optimization algorithm for mobility management in LTE-A and 5G HetNets," *IEEE Access*, vol. 8, pp. 294–304, 2020, doi: 10.1109/ACCESS.2019.2961186.

[16] M. U. B. Farooq, M. Manalastas, W. Raza, S. M. A. Zaidi, A. Rizwan, A. Abu-Dayya, and A. Imran, "A data-driven self-optimization solution for inter-frequency mobility parameters in emerging networks," *IEEE Trans. Cogn. Commun. Netw.*, vol. 8, no. 2, pp. 570–583, Jun. 2022, doi: 10.1109/TCCN.2022.3152510.

[17] R. Karmakar, G. Kaddoum, and S. Chattopadhyay, "Mobility management in 5G and beyond: A novel smart handover with adaptive time-to-trigger and hysteresis margin," *IEEE Trans. Mobile Comput.*, vol. 22, no. 10, pp. 5995–6010, Oct. 2023, doi: 10.1109/TMC.2022.3188212.

[18] N. A. E. Kuadey, G. T. Maale, T. Kwantwi, G. Sun, and G. Liu, "DeepSecure: Detection of distributed denial of service attacks on 5G network slicing—Deep learning approach," *IEEE Wireless Commun. Lett.*, vol. 11, no. 3, pp. 488–492, Mar. 2022, doi: 10.1109/LWC.2021.3133479.

[19] S. Kim, S. Kim, K. Suh, and B. Shim, "Action elimination-assisted deep reinforcement learning for B5G cell selection and network slicing," in *Proc. IEEE Global Commun. Conf. (GLOBECOM)*, Dec. 2022, pp. 3653–3657, doi: 10.1109/GLOBECOM48099.2022.10001669.

[20] C. C. González, E. F. Pupo, L. Atzori, and M. Murroni, "Dynamic radio access selection and slice allocation for differentiated traffic management on future mobile networks," *IEEE Trans. Netw. Service Manage.*, vol. 19, no. 3, pp. 1965–1981, Sep. 2022, doi: 10.1109/TNSM.2022.3150978.

[21] W. Tashan, I. Shayea, S. Aldirmaz-Çolak, O. A. Aziz, A. Alhammadi, and Y. I. Daradkeh, "Advanced mobility robustness optimization models in future mobile networks based on machine learning solutions," *IEEE Access*, vol. 10, pp. 111134–111152, 2022, doi: 10.1109/ACCESS.2022.3215684.

[22] X. Xu, Z. Sun, X. Dai, T. Svensson, and X. Tao, "Modeling and analyzing the cross-tier handover in heterogeneous networks," *IEEE Trans. Wireless Commun.*, vol. 16, no. 12, pp. 7859–7869, Dec. 2017, doi: 10.1109/TWC.2017.2754260.

[23] K. Vasudeva, M. Simsek, D. López-Pérez, and I. Güvenç, "Analysis of handover failures in heterogeneous networks with fading," *IEEE Trans. Veh. Technol.*, vol. 66, no. 7, pp. 6060–6074, Jul. 2017, doi: 10.1109/TVT.2016.2640310.

[24] M.-T. Nguyen and S. Kwon, "Geometry-based analysis of optimal handover parameters for self-organizing networks," *IEEE Trans. Wireless Commun.*, vol. 19, no. 4, pp. 2670–2683, Apr. 2020, doi: 10.1109/TWC.2020.2967668.

[25] T. A. Achhab, F. Abboud, and A. Assalem, "A robust self-optimization algorithm based on idiosyncratic adaptation of handover parameters for mobility management in LTE-A heterogeneous networks," *IEEE Access*, vol. 9, pp. 154237–154264, 2021, doi: 10.1109/ACCESS.2021.3127326.

[26] A. S. Priyadharshini and P. T. V. Bhuvaneswari, "Regression model for handover control parameter configuration in LTE-A networks," *Comput. Electr. Eng.*, vol. 72, pp. 877–893, Nov. 2018, doi: 10.1016/J.COMPELECENG.2018.01.011.

[27] *5G; NR; NR and NG-RAN Overall Description; Stage-2*, 3GPP Standard TS 38.300, Version 16.4.0, Release 16, 2021.

[28] C.-X. Wang, J. Bian, J. Sun, W. Zhang, and M. Zhang, "A survey of 5G channel measurements and models," *IEEE Commun. Surveys Tuts.*, vol. 20, no. 4, pp. 3142–3168, 4th Quart., 2018, doi: 10.1109/COMST.2018.2862141.

[29] T. S. Rappaport, G. R. MacCartney, M. K. Samimi, and S. Sun, "Wideband millimeter-wave propagation measurements and channel models for future wireless communication system design," *IEEE Trans. Commun.*, vol. 63, no. 9, pp. 3029–3056, Sep. 2015, doi: 10.1109/TCOMM.2015.2434384.

[30] S. Sun, T. S. Rappaport, T. A. Thomas, A. Ghosh, H. C. Nguyen, I. Z. Kovács, I. Rodriguez, O. Koymen, and A. Partyka, "Investigation of prediction accuracy, sensitivity, and parameter stability of large-scale propagation path loss models for 5G wireless communications," *IEEE Trans. Veh. Technol.*, vol. 65, no. 5, pp. 2843–2860, May 2016, doi: 10.1109/TVT.2016.2543139.

[31] *5G; NR; User Equipment (UE) Procedures in Idle Mode and in RRC Inactive State*, 3GPP Standard TS 38.304, Version 16.3.0, Release 16, 2021.

[32] *5G; NR; Requirements for Support of Radio Resource Management*, 3GPP Standard TS 38.133, Version 17.6.0, Release 17, 2022.

[33] *5G; NR; Base Station (BS) Radio Transmission and Reception*, 3GPP Standard TS 38.104, Version 17.7.0, Release 17, 2022.

[34] *5G; NR; User Equipment (UE) Radio Access Capabilities*, 3GPP Standard TS 38.306, Version 17.3.0, Release 17, 2023.

[35] B. Xie, Z. Zhang, R. Q. Hu, G. Wu, and A. Papathanassiou, "Joint spectral efficiency and energy efficiency in FFR-based wireless heterogeneous networks," *IEEE Trans. Veh. Technol.*, vol. 67, no. 9, pp. 8154–8168, Sep. 2018, doi: 10.1109/TVT.2017.2701356.

[36] J. G. Andrews, F. Baccelli, and R. K. Ganti, "A tractable approach to coverage and rate in cellular networks," *IEEE Trans. Commun.*, vol. 59, no. 11, pp. 3122–3134, Nov. 2011, doi: 10.1109/TCOMM.2011.100411.100541.

[37] *5G; NR; Physical Layer Procedures for Data*, 3GPP Standard TS 38.214, Version 16.2.0, Release 16, 2020.

[38] *5G; NR; Physical Layer Measurements*, 3GPP Standard TS 38.215, Version 15.7.0, Release 15, 2020.

ABBAS IBRAHIM MBULWA (Graduate Student Member, IEEE) received the M.Eng. degree in computer engineering from Universiti Malaysia Sabah (UMS), Kota Kinabalu, Malaysia, in 2019, where he is currently pursuing the Ph.D. degree in computer engineering. His research interests include next generation wireless communications, mobility management in heterogeneous networks, wireless ad hoc and sensor networks, and the Internet of Things.

HOE TUNG YEW (Member, IEEE) received the B.Eng. degree in electrical and electronic engineering from the University of Lincoln, Lincoln, U.K., in 2003, the M.Sc. degree in microelectronic and communications engineering from Northumbria University, Newcastle, U.K., in 2004, and the Ph.D. degree in biomedical engineering from Universiti Teknologi Malaysia, Skudai, Johor, Malaysia.

He is currently a Senior Lecturer with the Faculty of Engineering, Universiti Malaysia Sabah. He is a Chartered Engineer (CEng) with the Institute of Engineering and Technology, U.K., and a Professional Engineer with the Malaysia Board of Engineers. He has coauthored over 50 technical peer-reviewed journals and conference papers. His research interests include the general area of wireless communications and in particular in the area of vertical handover, wireless sensor networks, and the Internet of Things.

Dr. Yew served as the Executive Committee Member (Treasurer) for the IEEE Malaysia Sabah Subsection, from 2018 to 2020. He served as a TPC Member for the IEEE Malaysia Sabah Subsection conferences.

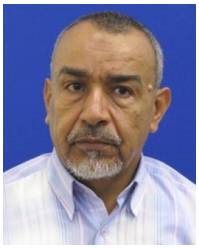

ALI CHEKIMA received the B.Sc. degree in electronic engineering from Ecole Nationale Polytechnique d'Alger (ENPA), Algeria, in 1976, and the M.Sc. and Ph.D. degrees in electrical engineering from the Rensselaer Polytechnic Institute, Troy, NY, USA, in 1978 and 1984, respectively.

He joined the Department of Electronics, ENPA, as an Assistant Professor, in 1984, where he was the Chairperson of the Scientific Committee, the Deputy of the Department of Electronics, and in charge of postgraduate studies. In 1995, he joined International Islamic University Malaysia, as an Associate Professor with the Department of Electrical and Computer Engineering. In 1996, he joined the School of Engineering and Information Technology (Now, Faculty of Engineering), University Malaysia Sabah. He became a Full Professor of computer engineering, in 2011. He has coauthored over 180 technical peer-reviewed journals and conference papers. His research interests include communication, pattern recognition, and artificial intelligence.

Prof. Chekima served as a TPC member for several international conferences.

JAMAL AHMAD DARGHAM (Senior Member, IEEE) received the B.Sc. degree in control and systems engineering from the University of Technology, Baghdad, Iraq, in 1984, the M.Sc. degree in control and systems engineering from The University of Manchester, U.K., in 1987, and the Ph.D. degree in computer engineering from Universiti Malaysia Sabah, Malaysia, in 2008.

From 1989 to 1996, he was a Lecturer with the Advanced Management College, Malaysia. In 1996, he joined the School of Engineering and Information Technology, now renamed as the Faculty of Engineering, Universiti Malaysia Sabah, where he is currently an Associate Professor. He was the Program Head of the Computer Engineering Program, from 2006 to 2011, and the Head of the Artificial Intelligence Research Unit, from 2016 to 2018. He has published more than 75 papers in refereed journals, conferences, book chapters, and research reports. His research interests include signal processing, image processing, biometrics, artificial intelligence, and engineering education.